White Rose Research Online

eprints@whiterose.ac.uk
https://eprints.whiterose.ac.uk
Universities of Leeds, Sheffield and York

Deposited via The University of Leeds.

White Rose Research Online URL for this paper:
https://eprints.whiterose.ac.uk/id/eprint/129978/

Version: Accepted Version

Article:
Gregory, LC, Mac Niocaill, C, Walker, RT et al. (2018) Vertical axis rotation (or lack thereof) of the eastern Mongolian Altay Mountains: implications for far-field transpressional mountain building. Tectonophysics, 736. pp. 31-46. ISSN: 0040-1951

https://doi.org/10.1016/j.tecto.2018.03.020

© 2018 Elsevier B.V. This manuscript version is made available under the CC-BY-NC-ND 4.0 license http://creativecommons.org/licenses/by-nc-nd/4.0/

Reuse
This article is distributed under the terms of the Creative Commons Attribution-NonCommercial-NoDerivs (CC BY-NC-ND) licence. This licence only allows you to download this work and share it with others as long as you credit the authors, but you can't change the article in any way or use it commercially. More information and the full terms of the licence here: https://creativecommons.org/licenses/

Takedown
If you consider content in White Rose Research Online to be in breach of UK law, please notify us by emailing eprints@whiterose.ac.uk including the URL of the record and the reason for the withdrawal request.

UNIVERSITY OF LEEDS
University of Sheffield
UNIVERSITY of York

Vertical axis rotation (or lack thereof) of the eastern Mongolian Altay Mountains: implications for far-field transpressional mountain building

Laura C Gregory[1*], Conall Mac Niocaill[1], Richard T Walker[1], Gantulga Bayasgalan[2] and Tim J Craig[3]

Affiliations

(1) University of Oxford, Department of Earth Sciences, South Parks Road, Oxford OX1 3AN, UK

**Present address: University of Leeds, School of Earth and Environment, Leeds LS2 9JT, UK, l.c.gregory@leeds.ac.uk*

(2) North Carolina State University, Department of Marine, Earth, & Atmospheric Sciences, Raleigh, NC 27695 USA

(3) University of Leeds, School of Earth and Environment, Leeds LS2 9JT, UK

Abstract

The Altay Mountains of Western Mongolia accommodate 10-20% of the current shortening of the India-Asia collision in a transpressive regime. Kinematic models of the Altay require faults to rotate anticlockwise about a vertical axis in order to accommodate compressional deformation on the major strike slip faults that cross the region. Such rotations should be detectable by palaeomagnetic data. Previous estimates from the one existing palaeomagnetic study from the Altay, on Oligocene and younger sediments from the Chuya Basin in the Siberian Altay, indicate that at least some parts of the Altay have experienced up to 39 ± 8° of anticlockwise rotation. Here, we present new palaeomagnetic results from samples collected in Cretaceous and younger sediments in the Zereg Basin along the Har-Us-Nuur fault in the eastern Altay Mountains, Mongolia. Our new palaeomagnetic results from the Zereg Basin provide reliable declinations, with palaeomagnetic directions from 10 sites that pass a fold test and include magnetic reversals. The declinations are not significantly rotated with respect to the directions expected from Cretaceous and younger virtual geomagnetic poles, suggesting that faults in the eastern Altay have not experienced a large degree of vertical axis rotation and cannot have rotated more than 7° in the past 5 m.y. The lack of rotation along the Har-Us-Nuur fault combined with a large amount of rotation in the northern Altay fits

with a kinematic model for transpressional deformation in which faults in the Altay have rotated to an orientation that favours the development of flower structures and building of mountainous topography, while at the same time the range widens at the edges as strain is transferred to better oriented structures. Thus the Har-Us-Nuur fault is a relatively young fault in the Altay, and has not yet accommodated significant rotation.

Key Words

Vertical axis rotation, strike slip faults, active faulting, palaeomagnetism, central Asian tectonics

1. Introduction

Where continental crust has structural fabric inherited from previous tectonic regimes, intracontinental mountain building is often accomplished by transpressional or transtensional deformation on structures that are not optimally oriented with respect to the regional stress field (Cowgill et al., 2004; Cunningham, 2005; Scholz et al., 2010; Walker and Jackson, 2004; Weil and Sussman, 2004). This occurs where pre-existing and un-favourably oriented structures are preferentially reactivated instead of developing new, optimally oriented faults. Vertical axis rotations (VAR) combined with strike-slip or oblique faulting plays an important role in accommodating the regional strain field in these intracontinental settings (e.g.Campbell et al., 2013; Cunningham, 2005; England and Molnar, 1990; Walker and Jackson, 2002). Investigating the kinematics of transpressional or transtensional mountain ranges is important for testing different models of continental deformation, such as whether deformation is distributed throughout the lithosphere or localised on major fault zones, and in understanding how large-scale continental strain is accommodated seismically (England and Molnar, 1990; Meade, 2007; Zuza and Yin, 2016). Quantifying the fault kinematics and the crustal rotations in these regions is crucial for reconciling modern-day strain rates derived from geodesy with Quaternary and longer fault slip rates.

The India-Eurasia collision provides an excellent natural laboratory for investigating distributed continental deformation. The Asian continent between the Siberian craton and the Indian plate was amalgamated in a series of collisions of microcontinents and fragmented arc complexes over hundreds of millions of years since the late Proterozoic (Badarch et al.,

1998; Badarch et al., 2002; Briggs et al., 2009; Cunningham et al., 2003b; Cunningham, 1998; Sengör et al., 1993). This long history has left several geologically complicated zones with strong inherited structural grain, which have been reactivated during the most recent collision with the Indian plate (Figure 1). These zones include the Kunlun, Qilian Shan, Tien Shan, Gobi Altay, Altay, Hanguy, and the Sayan mountain ranges.

The Altay Mountains of western Mongolia are located ~2500 km from the India-Asia suture (Figure 1). Despite being at the edge of the actively deforming regions, the Altay region accommodates 10 to 20% of the total shortening from the motion of India based on GPS velocities (Calais et al., 2006; Calais et al., 2003; Gan et al., 2007; Lukhnev et al., 2010; Wang et al., 2001; Yang et al., 2008; Zhang et al., 2004; Figures 1, 2). In contrast to the Himalaya and Tien Shan ranges further south, where shortening is predominantly accommodated by thrust faults oriented perpendicular and sub-perpendicular to the convergence direction (Abdrakhmatov et al., 1996; Molnar and Ghose, 2000), much of the deformation in the Altay is accommodated in a transpressive regime through slip on a rotating array of strike-slip faults (Baljinnyam et al., 1993; Bayasgalan et al., 2005; Walker et al., 2006).

A tenet of the style of deformation of the Altay is that the region rotates about a vertical axis in order to accommodate NNE—SSW directed shortening along right-lateral strike-slip faults that strike NNW—SSE (Baljinnyam et al., 1993; Bayasgalan et al., 2005). Figure 2b shows a schematic block diagram for rotation in the Altay, though in reality active deformation is distributed across the region on a complicated network of anastomosing faults mapped on Figures 1a and 3. Regional anticlockwise rotation is evident in the comparison between well-defined earthquake slip vectors and the direction of maximum horizontal strain vectors derived from GPS velocities across the mountains: slip vector azimuths are generally oblique to the principal strain axes and parallel to the NNW-striking active faults (Figure 3; Bayasgalan et al., 2005; Kreemer et al., 2014). While vertical axis rotation is a mechanism that can reconcile the geodetic and seismic data, few observations have been made on the longer term geological record of rotation in the region. Evidence of tectonic rotation on a geological time scale, including the amount and time-averaged rates of rotation, can be found by comparing palaeomagnetic declinations in older rocks to the predicted declination of the palaeomagnetic field at the time of deposition of those rocks. There is, however, only one previous study of Cenozoic palaeomagnetic directions in the Altay, conducted by Thomas et

al. (2002) on samples collected from the Chuya Basin in the Siberian Altay. Their results from Oligocene to Pleistocene clays and sandstones indicated significant anticlockwise rotations of 39 ± 8° over the past 40 Ma relative to a reference virtual geomagnetic pole (VGP) for Eurasia (Figure 3). Their study found dual-polarity and stable chemical remanent magnetisations, carried by magnetite, which are deviated with respect to the reference pole. They suggested that the measured rotation arises from left-lateral shear along the faults surrounding the Chuya Basin. Recent studies, however, have shown that these faults are, in fact, dextral strike-slip faults, as evidenced by the right-lateral 2003 M_w 7.2 Chuya earthquake (Nissen et al., 2007; Figure 1), indicating that the rotations result from the regional kinematics.

In order to contribute to the database of tectonic rotations in the Altay and to investigate the continuity of rotation across the region, we sampled Cretaceous to Pliocene sediments from the Zereg Basin for palaeomagnetic investigation (Figure 3). The Zereg Basin is formed in a transtensional bend in the Har-Us-Nuur fault, and is surrounded by several mountain ranges formed along restraining bends in the fault system (Figures 3 & 4). The relief surrounding the Zereg Basin is relatively young, uplifted only within the last 3—8 Ma on the basis of low-temperature thermochronology studies (Jolivet et al., 2007). There are several motivations for selecting the Zereg Basin as a palaeomagnetic study locality. Appropriate material for palaeomagnetic study is limited in the Altay, and the Zereg Basin is a locality where extensive uplifted Jurassic and younger-aged sediments are preserved (Howard et al., 2003). Good age constraints are also required to interpret palaeomagnetic directions, and in the Zereg Basin stratigraphic ages have previously been determined by several authors (Devyatkin et al., 1975; Howard et al., 2003; Khosbayar, 1973; Shuvalov, 1968, 1969; Sjostrom et al., 2001). Whilst local basin-scale rotations can often overprint the regional rotations that are the focus of this study, the structural evolution of the Zereg Basin is well known based on the excellent exposure of active faults, folds, and uplifted stratigraphic units, and can therefore be corrected for in palaeomagnetic data by restoring sample directions to their tilt-corrected orientations.

The degree of Cenozoic rotation along the Har-Us-Nuur fault in the Zereg Basin can also be used to test the age of initiation of faulting and mountain building, given assumptions about how these rates relate to rotation. For example, if the fault bounding the Zereg Basin is relatively young, small amounts of rotation may be expected. Finally we discuss these results

in the context of an actively evolving transpressional mountain range and the hazard presented by the strike slip faults.

2. Geological Background

2.1 Regional setting

Deformation in the Altay is accommodated primarily on a distributed network of long strike-slip faults oriented NNW–SEE, which is oblique to the NNE–SSW oriented maximum shortening direction (Figure 3). Faults follow the dominant structural grain imposed by Palaeozoic deformation during the assembly of central Asia, during which the Altay region was a continental arc setting accreted on the margins of the Siberian craton (Badarch et al., 1998; Badarch et al., 2002; Briggs et al., 2009; Cunningham et al., 2003b; Cunningham, 1998; Sengör et al., 1993). These faults have accumulated several kilometres of right-lateral displacement and are capable of producing up to M_w 8 earthquakes, as shown by historic and prehistoric examples (Baljinnyam et al., 1993; Klinger et al., 2011; Figure 1). A limited number of Quaternary fault slip rates have been determined for the major Altay faults and they range between 0.5–2.5 mm yr^{-1}, with the most rapid rates found on the eastern-most structure: the Har-Us-Nuur fault (Figure 3; Frankel et al., 2010; Gregory et al., 2014; Nissen et al., 2009a; Nissen et al., 2009b). Given the slow time-averaged rate of slip on faults in the Altay, large earthquakes have long recurrence intervals, and any individual fault may have over 1000 years between significant events.

The cold arid climate of Mongolia allows for good preservation of faulting and deformation features in the landscape, such as pre-historic earthquake ruptures and cumulative Quaternary fault displacements (Baljinnyam et al., 1993; Nissen et al., 2009b; Walker et al., 2006). Also, the high topographic relief of the Altay potentially preserves the total vertical uplift due to Cenozoic deformation, based on the assumption that ancient planation surfaces have been uplifted and preserved without significant erosion on the tops of many mountains (e.g. Jolivet et al., 2007). The highest mountain peaks in the Altay reach over 4000 m, and the region has a high average elevation (~2300 m, Baljinnyam et al., 1993). This is in part due to the elevation of the intervening basins, which are between 1500 and 2500 m in elevation, and thus the overall topographic relief in the range is generally on the order of 2000 m.

Conflicting low temperature thermochronology results suggest that the western Altay may have experienced tectonic activity from the early Miocene (~25-20 Ma, Yuan et al., 2006), while workers in the eastern Altay and the Siberian Altay suggest that the full onset of Cenozoic deformation, which has produced the present-day relief in the Altay, did not begin until more recently (having been initiated within the last 8 Myr; De Grave and Van den haute, 2002; De Grave et al., 2008; Glorie et al., 2012a; Glorie et al., 2012b; Jolivet et al., 2007; Vassallo, 2006; Vassallo et al., 2007). These authors suggest that the modelled cooling ages from low-temperature chronology is evidence of the onset of the currently active deformation regime due to the preservation of peneplain surfaces on average ~2000 m above the valley floors, which represents the total uplift in the region due to compression from the India-Asia collision. Sedimentation records in the basins surrounding the Altay are consistent with some regional uplift following at least the Oligocene, or ~23 Mya. Sedimentary basins on the eastern margin of the Altay have an Oligocene unconformity, which is overlain by Miocene aged debris-rich fluvial sedimentary units (Cunningham et al., 2003a; Cunningham, 2011; Howard et al., 2003). An increase in conglomeritic deposits in the Plio-Pleistocene in the eastern Altay basins suggest an overall increase in tectonism or that uplift is more proximal to the eastern Altay during the past 5 Myr.

The right-lateral faulting in the Altay is in contrast to the faulting directly east of the Altay in the Gobi Altay and along the Bulnay fault zone, where GPS vectors are directed east-west and parallel to the large sinistral faults, requiring no rotation (Figures 1 & 2). The generally NNW–SSE trend of the structural grain in the Mongolian Altay gradually bends to strike E–W in the Gobi-Altay, parallel to the Bulnay fault to the north. The E–W faults are suggested to accommodate the space problem created by rotation in the Altay (Figure 2b; Bayasgalan et al., 2005) as well as a switch to left-lateral shear and eastward motion of central Mongolia with respect to stable Eurasia (Walker et al., 2007).

Figure 1

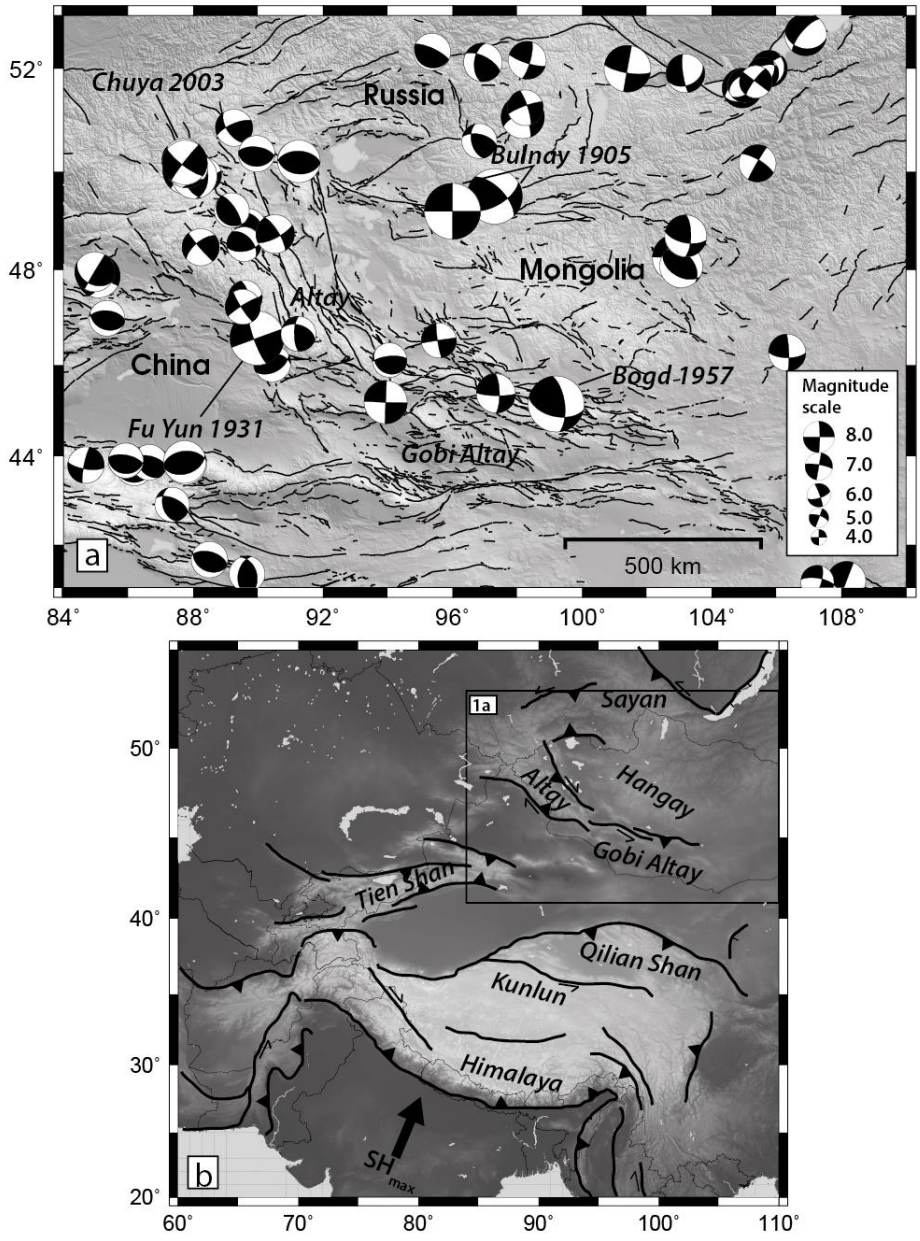

176

177 **Figure 1**: (a) SRTM shaded relief image of the Altay and (b) the India-Asia collision zone,
178 produced using the Generic Mapping Tools software (GMT, Wessel et al., 2013). In (a)
179 earthquake focal mechanisms are from Sloan et al. (2011), Nissen et al. (2007), and
180 Bayasgalan et al. (2005, other references within), with $M_w > 7$ events indicated. Active faults
181 are plotted in black (Baljinnyam et al., 1993; Gregory, 2012). (b) SRTM topography and major
182 tectonic boundaries of the India-Eurasia collision.

183

Figure 2

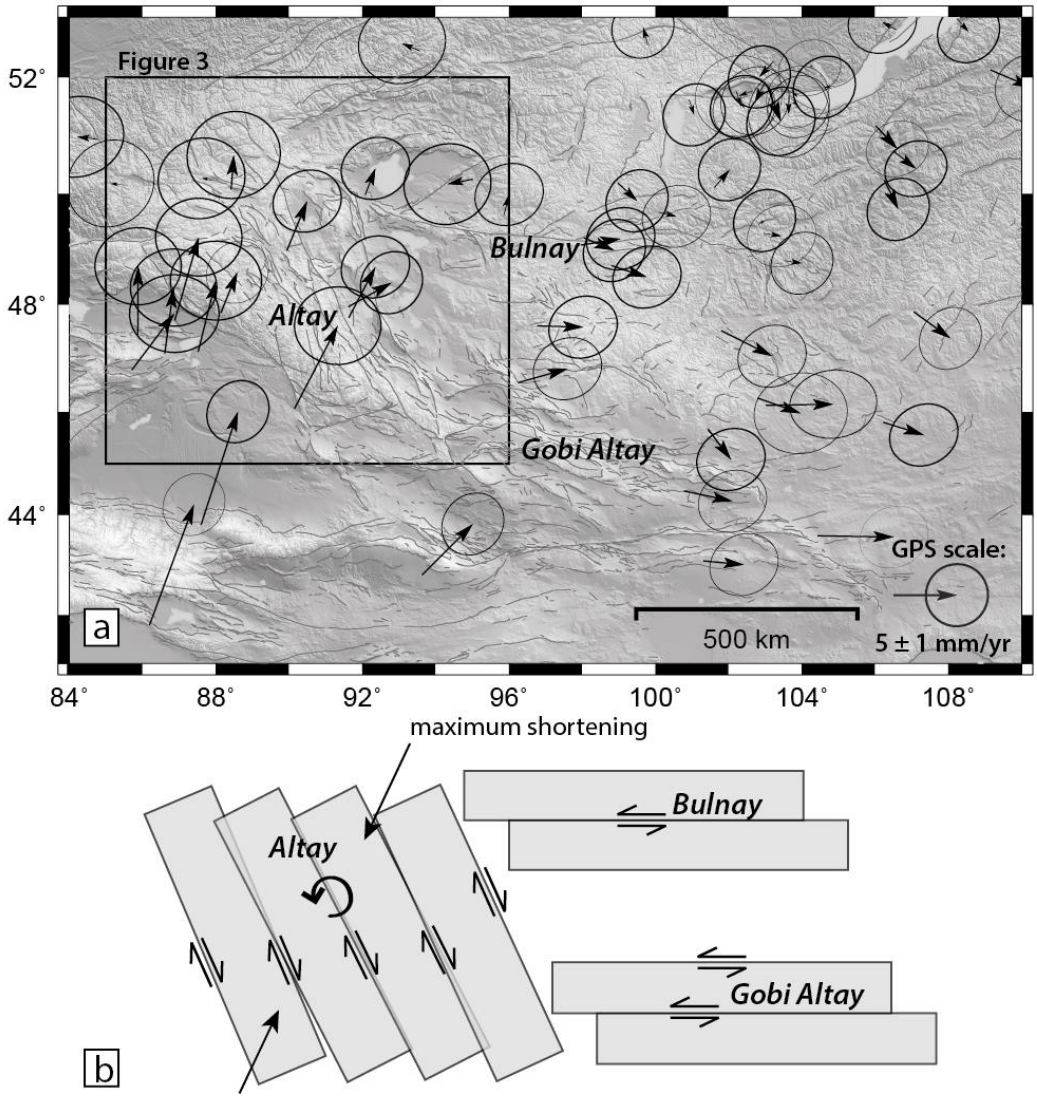

184

185 **Figure 2:** (a) SRTM shaded relief image of the Altay. GPS velocities are relative to stable
186 Eurasia and suggest ~7 mm yr^{-1} of northeast-directed shortening across the Altay (Calais et
187 al., 2006; Yang et al., 2008). Active faults are plotted in grey (Baljinnyam et al., 1993; Gregory,
188 2012). (b) Schematic diagram for deformation in Mongolia, with rotation on dextral faults in
189 the Altay (W Mongolia), and non-rotational shear required across the Gobi Altay and central
190 Mongolia, following the pattern of GPS-derived velocity vectors plotted in (a). In this
191 kinematic model, *w* indicates the average spacing between faults and θ is the degree of
192 rotation for an amount *d* of fault displacement after Walker and Jackson (2004) and described
193 in section 5.2.

Figure 3

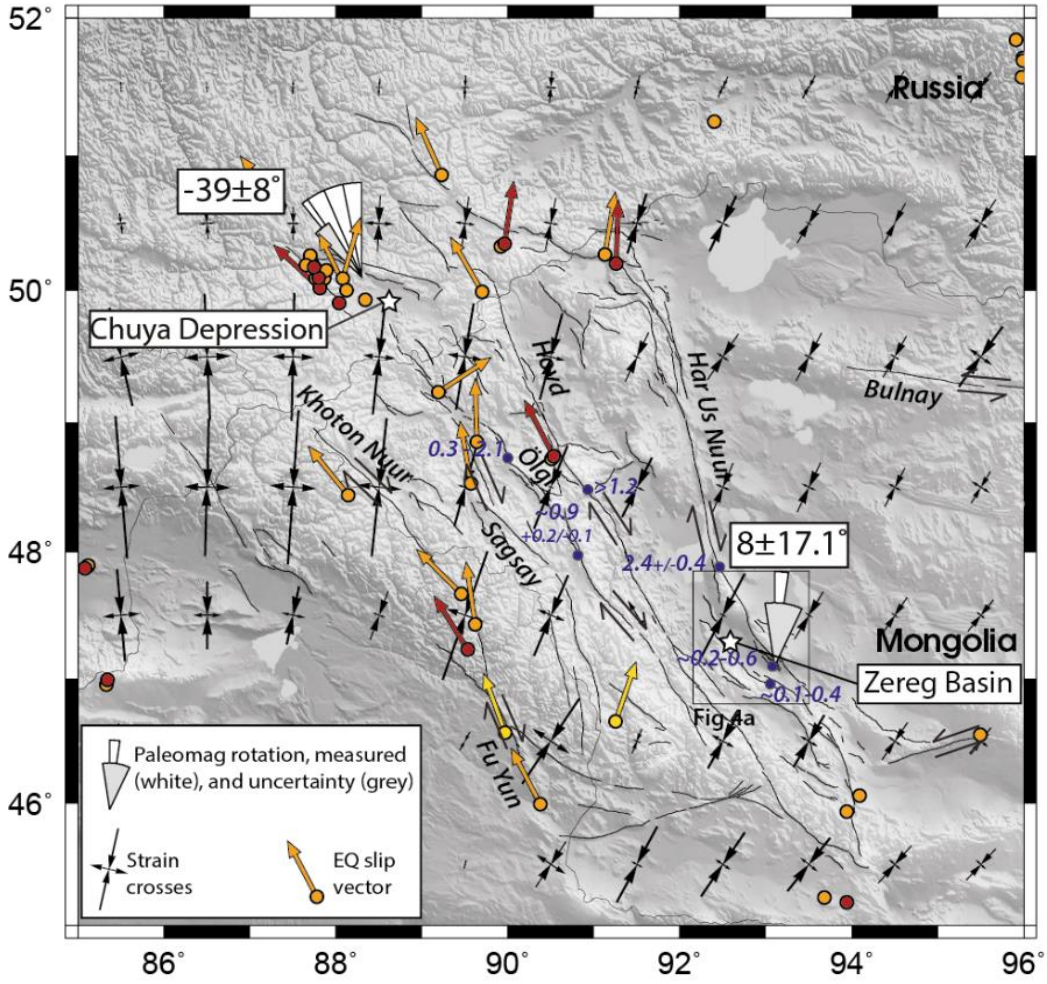

194

195 **Figure 3:** Map of the Altay Mountains and active strike-slip faults. Black strain crosses show
196 the principal strain axes (compressional arrows point in, extensional arrows point out) from
197 Kreemer et al. (2014). Quaternary slip rates are noted in blue from Frankel et al. (2010);
198 Gregory et al. (2014); Nissen et al. (2009a); Nissen et al. (2009b); and Vassallo (2006). Rotation
199 estimates are plotted as rotational wedges in radians from north (white) with uncertainties
200 (grey) for the Chuya Basin (Thomas et al., 2002) and Zereg Basin (this study, each wedge
201 division is 2 radians). Coloured dots (earthquake locations) and arrows (earthquake slip
202 vectors) are for first-motion mechanisms (yellow; Bayasgalan et al., 2005, and references
203 therein), waveform-modelled solutions (red; Sloan et al., 2011, and references therein), and
204 from the Global CMT Catalogue (orange). Earthquake slip vectors are only plotted where the
205 fault plane is reliably established by field or remote mapping of the active trace. Where
206 discrimination between the fault and auxiliary plane is not possible, no slip vector is plotted.

2.2 Stratigraphy and structural geology of the Zereg Basin

The Zereg Basin lies between transpressional massifs formed along the Har-Us-Nuur fault, which is the easternmost of the major faults in the Altay (Figure 3). The bedrock exposed in the surrounding mountains comprises Vendian and Palaeozoic metasedimentary and volcanic basement that was intruded by granitic plutons in the Palaeozoic (Devyatkin, 1981; Howard et al., 2003). The Zereg Basin was initially formed as an extensional half-graben during the Jurassic-Cretaceous, and was later reactivated as a transpressional basin in the current tectonic regime (see Figure 15 in Howard et al., 2003). The basin is approximately 140 km long and ranges from 20 to 30 km wide. The Zereg Basin and surrounding mountains are the site of several key studies in the Altay, including Quaternary slip rate studies in Nissen et al. (2009a) and Nissen et al. (2009b), and investigations of the Mesozoic and Cenozoic stratigraphy and structure of the basin and active faults (Cunningham, 2007; Cunningham et al., 1996; Howard et al., 2003; Sjostrom et al., 2001). Continuous outcrops of Mesozoic and Cenozoic strata are exposed in incised drainages along the range fronts of the Jargalant, Bumbat, and Baatar Hyarhan mountains, uplifted by active thrust faults that have propagated into the basin (e.g. Nissen et al., 2009a).

Figure 4

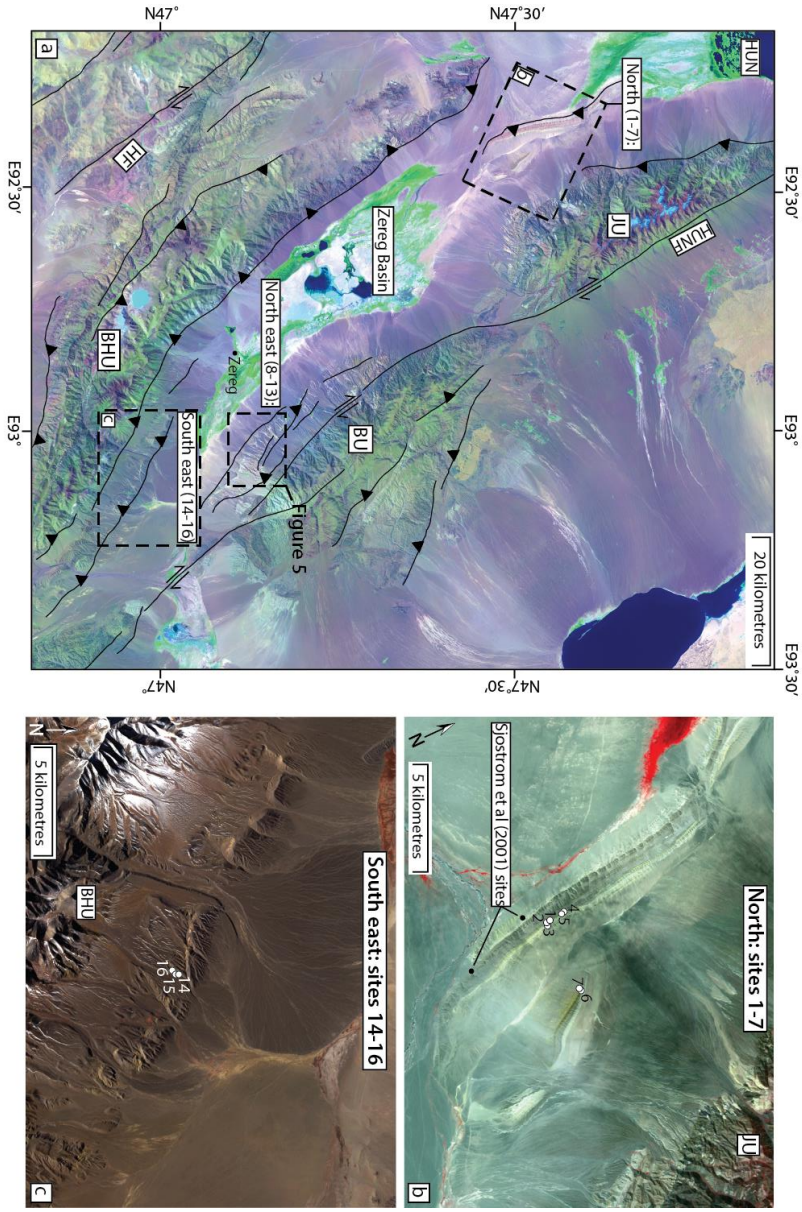

Figure 4: (a) Landsat image (RGB = 741) of the Zereg Basin, with the three different sampling localities indicated (North, North east, and South west). Figure 4 is indicated by dashed box. Abbreviations are BHU: Baatar Hyarhan Uul, BU: Bumbat Uul, HF: Hovd Fault, HUN: Har-Us-Nuur, HUNF: Har-Us-Nuur Fault, and JU: Jargalant Uul. The town of Zereg is indicated. (b) and (c) are ASTER images of the northern and south-western sampling localities, with sample sites labelled.

Figure 5

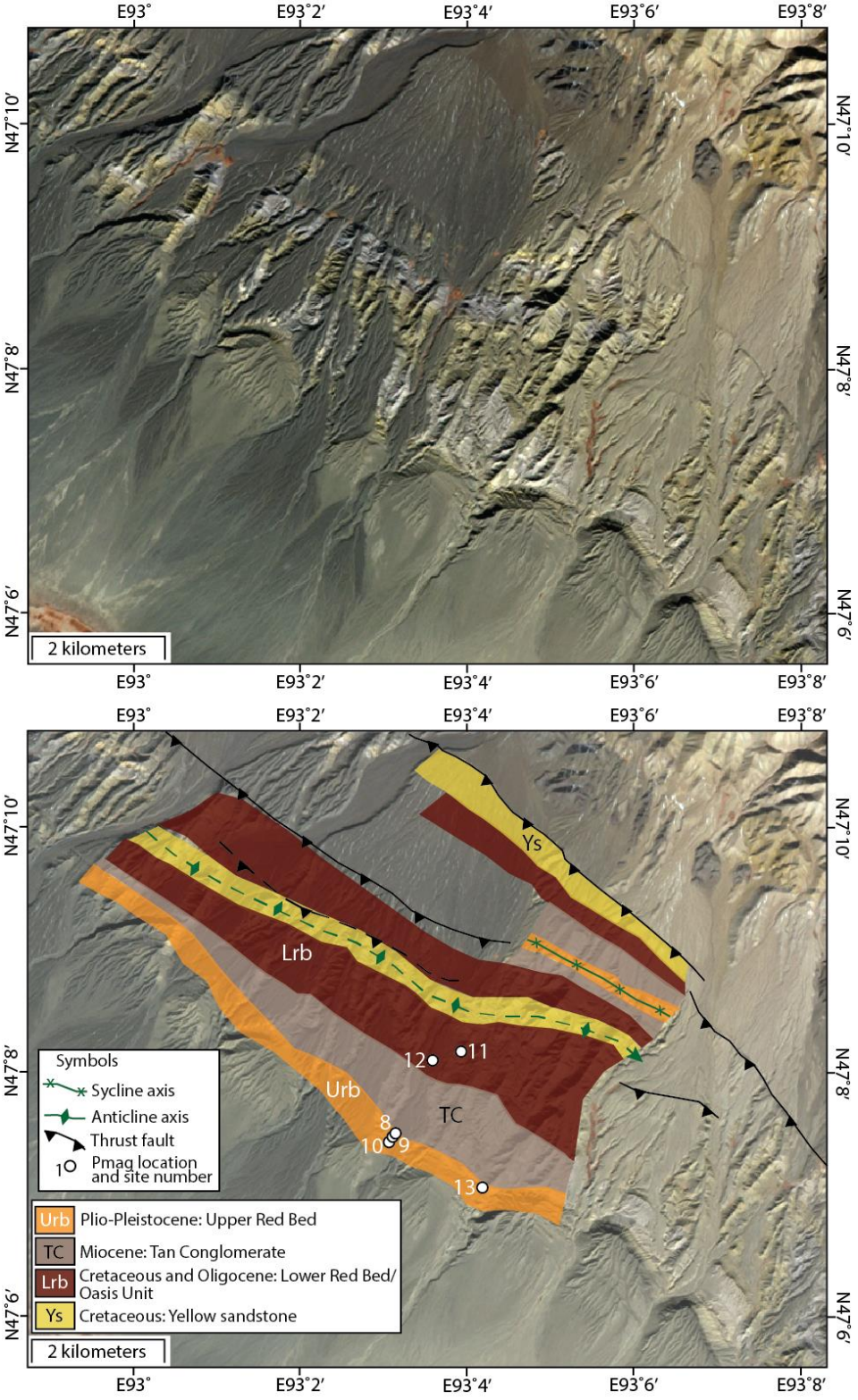

230

231 **Figure 5**: ASTER imagery (15 m/pixel) of the sampling sites from the northeast side of the
232 Zereg Basin. The lower panel shows a geological map of the area modified from Howard et al.
233 (2003) and (Nissen et al., 2009a), with the ages of the units mapped labelled and sampling
234 localities indicated. The region includes a syncline-anticline pair.

We briefly summarise the stratigraphy of the sampled sections summarised here based on our observations and previous work. Sjostrom et al. (2001) investigated the sedimentology and provenance of Mesozoic strata and Howard et al. (2003) describe the stratigraphic and structural evolution of the Zereg Basin, both based on extensive field work and previously published palaeontologic work from the Russian literature for the relative dating of sedimentary units (Devyatkin, 1981; Devyatkin et al., 1975; Khosbayar, 1973; Shuvalov, 1968, 1969). We targeted units in the Zereg Basin that had been previously investigated in order to have sufficient age control for our palaeomagnetic analyses.

The oldest sediments in the Zereg Basin are Jurassic red conglomeritic sandstones, which underlie the sequence and are exposed at the Oshin Nuruu site described by Sjostrom et al. (2001). These are overlain by the oldest named unit in the sequence, the Yellow Sandstone Unit, which is early Cretaceous in age on the basis of fossils belonging to phylum *Mollusca*, class *Ostracoda*, fishes, and a small ornithischian dinosaur (Devyatkin et al., 1975; Howard et al., 2003; Khosbayar, 1973). The Yellow Sandstone Unit is 150 m thick and comprises red pebbly conglomerates below interbedded grey siltstone and buff-coloured sandstone with typically erosive bed bases. Howard et al. (2003) interpreted the unit to represent at the base a lacustrine setting overlain by a succession of sheet floods. They suggest that the top of the unit represents a shallow sand-bed river system deposited in an alluvial setting during a drop in lake level. This unit is exposed on the southwest flanks of Jargalant Mountain, uplifted along two thrust faults developed in the flower structure associated with the restraining bend in the Har-Us-Nuur fault (Figure 4a 'North' box shown in detail in Figure 4b, sampling localities 1-7). The Yellow Sandstones are overlain by the up to 450 m thick Lower Red Bed Unit, which is also early Cretaceous (Albian-Aptian) in age on the basis of *Mollusca*, *Ostracoda*, and *Insecta* fossil assemblages (Devyatkin et al., 1975). This unit is characterised by alternating red and grey siltstones with red sandstones. The Lower Red Bed environment is interpreted as periodic inundation of a floodplain or distal alluvial fan setting, deposited from suspension in standing water (Howard et al., 2003). Palaeomagnetic sites 1-7 were sampled from both the buff-coloured sandstones and finer grained layers in the red conglomeritic sandstone in the Jurassic-Cretaceous succession at Oshin Nuruu (Figure 4b).

There is an angular unconformity between the Lower Red Beds and the ~140 m thick Oligocene Oasis Unit (Howard et al., 2003). The prevalence of micromammalia establish the

Oligocene age of the unit (Devyatkin, 1981). This unit consists of interbedded sandstones and siltstones, with frequent calcium carbonate concretions near the top of the sequence. The unconformity at the base of the Oasis Unit is thought to represent a period of tectonic quiescence and the formation of the early Cenozoic planation surface preserved across the eastern Altay and Gobi Altay. This unit is also thought to originate as part of a distal alluvial fan system that had plenty of accommodation space, based on the lack of evidence for aggradation in channels (Howard et al., 2003). The carbonate concretions may represent extensive caliche development associated with alluvial fan abandonment. We collected sites 11-12 from the Oasis unit in fine sandstones and red siltstones, location shown in Figure 5.

Miocene-aged sediments are present in the Zereg Basin, but these were too coarse grained for palaeomagnetic analyses and we do not describe them in detail. The overlying sequence comprises the Pliocene –Lower Pleistocene Upper Red Bed, Upper Yellow Conglomerate, and Grey Conglomerate units (Howard et al., 2003). The Pliocene Upper Red Beds are conformable with the Miocene sequence, and mostly comprise interbedded, fining-upwards and red-stained conglomerates and siltstones. This unit is exposed on the northeast and southern sides of the basin, though on the southern side it is referred to as the Upper Yellow Conglomerate Unit by Howard et al. (2003). The Plio-Pleistocene sequence is coarser than underlying sequences, and represents the most recent phase of tectonism in the surrounding mountains. Massive beds with vertical grading indicate the sequence was deposited in a braided stream fluvial or alluvial environment, and evidence of debris flow flooding is occasionally present in clast-supported conglomerate layers (Howard et al., 2003). The Upper Red Beds/Yellow Conglomerate Units are dated as Pliocene based on mammal fossils and fresh water molluscs (Devyatkin, 1981; Howard et al., 2003). Sites 8-10, and 13 on the north east site of the basin and sites 14-16 on the south side of the basin are collected from the most consolidated and fine grained layers within Upper Red Beds (locations indicated on Figures 4a, c, and 5).

Figure 6

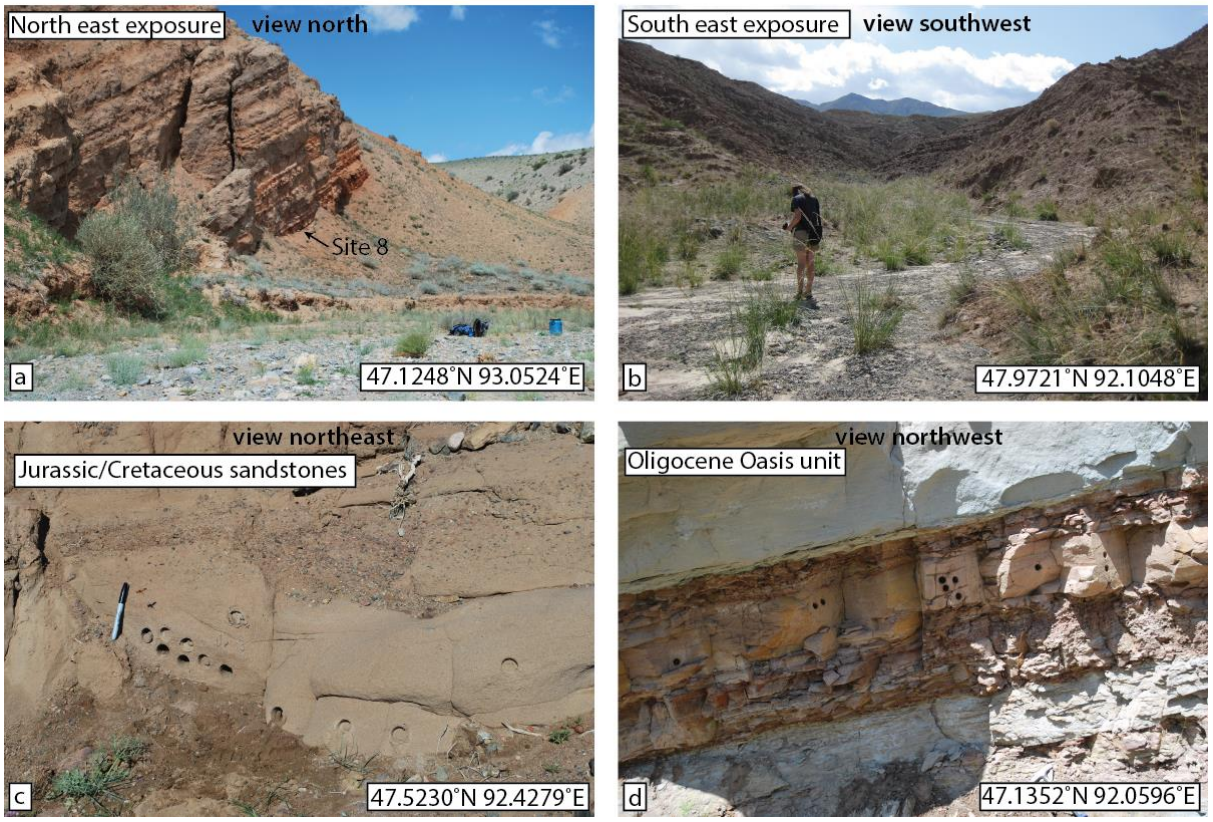

Figure 6: Photos of the exposures of Cenozoic and Mesozoic sediments in the northeast and southeast Zereg Basin. (a) Outcrop of the upper red-bed unit, with strata uplifted by southwest-dipping thrust faults (site 8). (b) Upper Red Bed Plio-Pleistocene sediments uplifted on the flanks of Baatar Hyarhan Mountain, dipping SW towards the peaks of Baatar Hyarhan in the background (sites 14-16). (c) Cretaceous sandstones with palaeomagnetic drill holes at site 6. (d) Oligocene Oasis Unit, with interbedded red sandstones (sampled, site 12) and yellow sandstones with cross bedding.

Palaeomagnetic methods

3.1 Sampling strategy

Oriented palaeomagnetic cores were collected from 16 sites in three different regions of the basin (Figure 4, 6). The three stratigraphic sections sampled are uplifted along different strands of the faults surrounding the Zereg Basin, and as a result, have distinguishable tectonic orientations. Sampling from the same units over a variety of structural orientations adds confidence to the palaeomagnetic results, not only by producing duplicate samples of the same unit in different areas, but also because the sampling strategy helps to determine

whether local, fault-related rotations have affected the results. If local rotations have occurred, corrected sample directions from sites of the same age will not necessarily agree across the different sampling localities. The three sampling localities cover the length and width of the basin, and were specifically chosen because each locality has well-constrained Cretaceous and younger stratigraphy.

The Jurassic-Cretaceous Oshin Nuruu site on the southwest flanks of Jargalant Mountain was targeted for the northern-most palaeomagnetic sampling site in this study (sites 1—7 in Table 1, Figures 4b, 6c). There are two separate exposures uplifted on what were suggested by Cunningham et al. (1996) to be two splay thrust faults related to the main Jargalant faults. The palaeomagnetic sites for analysis were collected from stratigraphically above the Jurassic sections in Jurassic to Cretaceous aged red conglomeratic sandstone units and grey to yellow coarse-grained sandstone units. Sites 1—5 were collected from the sediments uplifted by the western-most thrust fault, and sites 6 and 7 from the units uplifted by the eastern thrust (Figure 4b). Samples were collected from finer grained mudstone and siltstone units interbedded with the conglomerates. Sediments on the eastern ridge are coarser grained, including 1—2 mm sized pebbles within much of the sandstone and mudstone units, and were less consolidated than those from the western ridge.

Sites 8 through 13 were collected from Cenozoic strata uplifted in the range front of Bumbat Mountain (Figure 5, 6a). The sites are part of a thrust fault driven syncline-anticline pair that has folded Upper Jurassic to Plio-Pleistocene sediments, which are unconformably overlain by Quaternary alluvial fans. A similar sedimentary sequence is also uplifted on the opposite side of the Zereg Basin, where sites 14—16 were collected (Figure 4a, 4c, 6b). No major folds were identified where we sampled on the southwest side of the Zereg Basin, and the succession consistently dips southwest towards Baatar Hyarhan Mountain.

The Cretaceous and younger stratigraphy is divided into four groups: the Cretaceous Lower Red Beds, the Oligocene Oasis Unit, the Miocene Tan Conglomerates, and the Pliocene Upper Red Bed/Pleistocene Conglomerates (Howard et al., 2003; Figure 5b). Two palaeomagnetic sites were collected from the Oasis Unit (sites 11–12), stratigraphically above the unconformable boundary with the Cretaceous Lower Red Beds (Figure 6d). Several sites were sampled from the Pliocene Upper Red Bed Unit on both the north-eastern and south-eastern

side of the Zereg Basin. The sediments sampled on the south-eastern side of Zereg (sites 14-16) were similar in colour, sorting, grain size, and stratigraphic relationships between interbedded layers to those sampled on the north-eastern side of the basin (sites 8-10 and 13) in the Upper Red Bed Unit, confirming that the same unit is represented on both sides of the basin. All sites were sampled in finer grained and more consolidated layers as these are more reliable for palaeomagnetic analyses. We collected samples from specific localities that had previously determined age constraints as described in section 2.2 and published in Devyatkin (1981); Howard et al. (2003); and Sjostrom et al. (2001).

3.2 Palaeomagnetic sampling techniques and experiments

Samples were collected in the field using a gasoline powered hand drill, and were oriented with a magnetic compass. Due to the low magnetic intensity of the sediments, no correction for magnetic interference from the outcrop was necessary. Over 160 core samples were collected from 16 sites in three different regions of the Zereg Basin (Figure 4, Table 1). Samples were carefully wrapped in the field and further processing was done at the University of Oxford palaeomagnetic laboratory. Core samples were cut into standard sized specimens using a custom saw, and a few delicate samples were cut by hand with a utility knife and then sanded to remove any possible metal contamination from the knife. Samples were stored and measured in a magnetically shielded room, with an internal field <200 nT. A pilot batch of 1-2 specimens from each site was thermally step-wise demagnetised at temperature intervals of 50°C steps up to 500°C, followed by 20°C steps to 620°C, and then by 10°C steps until demagnetised (up to about 700°C). After analysing the preliminary samples, a series of thermal steps up to 700°C were chosen for demagnetisation of the remaining samples (generally at 60°C steps to 540°C, followed by 20°C steps to 700°C). Magnetic measurements were made on samples in between each heating step, on the Oxford 2-G enterprises Model 755 3-axis cryogenic magnetometer. Best-fit magnetic components found during demagnetisation were determined for linear segments on orthogonal plots, using the least-square regression analysis implemented in the Super IAPD program (http://www.geodynamics.no/software.htm). The orthogonal plot is a display of the horizontal and vertical (declination and inclination) projection of the magnetisation scaled with intensity at each temperature step (Figure 7; Zijderveld, 1967).

368 *3.2 Rock magnetic experiments*

369 In order to better characterise the carriers of magnetisation in samples, magnetic tests were
370 performed on samples. Initial susceptibility was measured for all samples, and Curie
371 temperature measurements were carried out on a select group of powdered samples
372 (representing the variety in age and composition in the sampling sites) using a KLY-2
373 susceptibility bridge with a CS2 heating unit (Figure 8). In these experiments, the susceptibility
374 of a finely crushed sample is incrementally measured during heating and cooling. The
375 magnetic carrier can be determined from the change in magnetic susceptibility with
376 temperature, in particular the value for the Curie temperature of the sample, which occurs
377 when the magnetic ordering is destroyed with an accompanying loss of susceptibility (e.g.
378 Merrill et al., 1998).

379 **4. Results**

380 *4.1 Palaeomagnetic data*

381 Palaeomagnetic data from sites that have consistent and stable remanent magnetisations are
382 listed in Table 2. Representative orthogonal plots and thermal demagnetisation paths are
383 displayed in Figures 6a, b, and c from the three different regions of the Zereg Basin shown in
384 Figure 4. The intensities of natural remanent magnetisations (NRM) range from around 1 to
385 44 mA/m, with generally lower intensities in samples that had less stable directions. Site
386 averaged NRM intensities for sites used in our analyses are listed in Table 2. The highest
387 intensities were found from a site that yielded inconsistent directions and has not been
388 included in the analysis (site 9). A low coercivity component was frequently removed from
389 samples at lower temperatures (up to ~250°C), which can generally be attributed to the
390 present day field (north and steep, e.g. Figure 7), possibly as a result of recent weathering.
391 Many samples lost a significant percentage of intensity at temperatures up to approximately
392 120°C, which may be indicative of the presence of goethite imparting a chemical remanent
393 magnetisation (CRM, e.g. sample M912-1, Figure 7). However, once this low coercivity
394 component was removed, a stable magnetic direction could generally be found from the
395 higher temperature measurements (e.g. sample M916-3, Figure 7). Samples were fully
396 demagnetised when the intensity of magnetisation is less than 10% of the NRM. Full
397 demagnetisation occurred at high temperatures between 560—700°C, indicating that both

magnetite and hematite may be contributing to the primary magnetisation in the samples that did not fully demagnetise at 580˚C, as the Curie temperatures are 580°C for magnetite and between 675° to 725°C for hematite (Merrill et al., 1998).

Both *in-situ* and tilt-corrected directions for the stable high coercivity components are listed in Table 2 and shown in Figure 9. The tilt correction was made for each site based on the strike and dip of the strata sampled (Table 1). In order to test for tectonic rotation of the samples as well as inclination flattening during compaction, the tilt-corrected directions can be compared to the expected VGP (virtual geomagnetic pole) for the time of deposition. VGPs were calculated from the apparent polar wander path (APWP) for Eurasia catalogued by Torsvik et al. (2012) for the Zereg Basin using the GMAP2003 program (available at http://www.geodynamics.no/software.htm). The degree of rotation for each site is the difference between the measured tectonic corrected declination (D_{tc}) and the expected declination for a given stratigraphic age based on the VGP. The flattening of a site is the difference between the expected inclination and tilt-corrected, measured inclination (I_{tc}).

Uncertainties at the 95% confidence level for the rotation and flattening were determined following methods in Demarest (1983). Uncertainties are based in part on classic Fisher (1953) statistics for the probability distribution of a two dimensional cone of 95% confidence (α_{95}). A small correction factor is added to the uncertainty, in line with Demarest (1983), which takes into account the precision of the results as well as the inclination of samples. The uncertainties for rotation of declinations increase as inclinations steepen, and as inclination approaches 90°, a range of 0—360° for declination is possible.

Figure 7

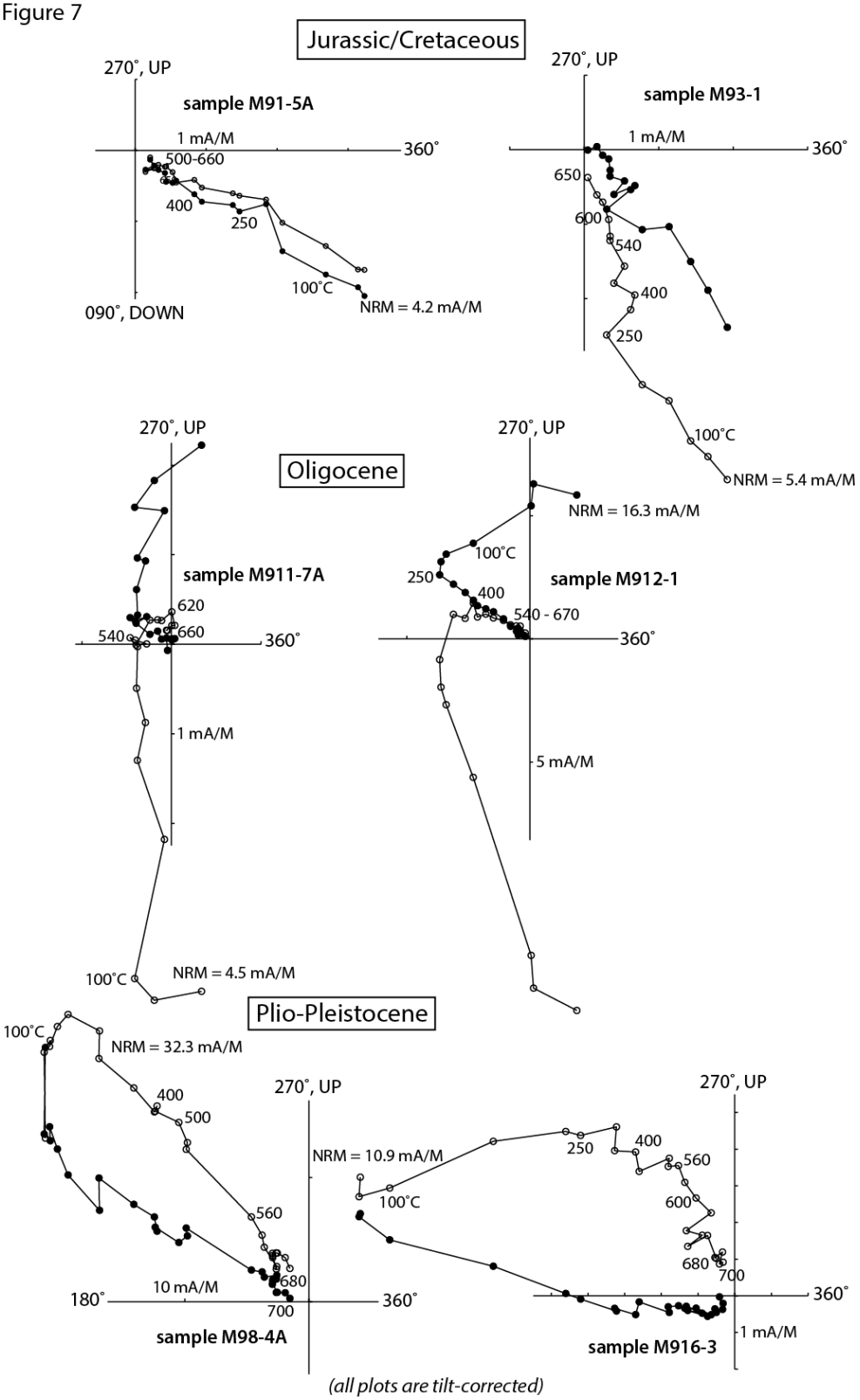

Figure 7: Example thermal demagnetisation Zijderveld diagrams from each rock unit sampled. Plots are shown tilt-corrected with a tectonic correction for the orientation of the strata sampled. Open points indicate the inclination, and closed points are the sample declination.

North is to the right of the plot, and magnetic declinations are fit as vectors through measurements from high to low temperature.

Rotations of individual sites from the expected VGP declination are between 22° clockwise to 6° anticlockwise. The site rotations are combined into groups based on their stratigraphic age. The majority of samples yield inclinations that are shallower than those predicted from the reference poles by >10°, and have likely experienced inclination flattening. This shallowing phenomenon is common amongst sedimentary rocks due to compaction, particularly in Cenozoic sediments in central Asia, where sedimentary samples are reported to have inclinations that are 20° shallower than expected (Dupont-Nivet et al., 2002; Tauxe and Kent, 2004; Thomas et al., 1993). The majority of sites in the Zereg Basin have experienced inclination shallowing of approximately equal to or less than 20°. The exceptions to this are sites 1, 11, and 12, which have experienced significantly more flattening. However, the shallowing of inclinations does not affect the sample declination, and shallowing may also support a primary magnetisation because it is suggested to be acquired during and immediately following sedimentary deposition (Tauxe and Kent, 2004).

4.2 Magnetic tests

The results of susceptibility tests are shown in Figure 8, for select sites that have stable demagnetisation vectors as well as one site with inconsistent directions (site 9). Samples from sites 3, 9, and 11 display a characteristic *Hopkinson* effect, which is an increase in susceptibility just before the Curie temperature drop in susceptibility, and is often associated with the unblocking temperature of the magnetisation (e.g. Tauxe, 2010). The loss of susceptibility around 560°C is characteristic of magnetite being the primary carrier of magnetisation, and most samples display a drop in susceptibility in this range. Some samples also lose the remaining susceptibility around 680—700°C, suggesting that haematite is also present in those samples.

In some cases, the statistics of the mean directions from a site are quite poor, with high α_{95} values and low k (kappa) values. Whilst there is no specific acceptable standard for α_{95} and k, values of $\alpha_{95} < 16$ and $k > 10$ are considered to be typical for good quality studies (e.g. Van der Voo, 1989). Two sites yielded α_{95} values > 16: sites 3 & 6. At site 3 the high α_{95} can be attributed to the low number of specimens, and they yield a perfectly acceptable value of k.

At site 6 both the α_{95} value and k lie marginally outside the Van der Voo (1989) criteria, due to the low magnetic intensity of the specimens. Site 14 yield too few stable directions to calculate statistics, but the mean direction nonetheless agrees with that from other sites at that locality.

Figure 8

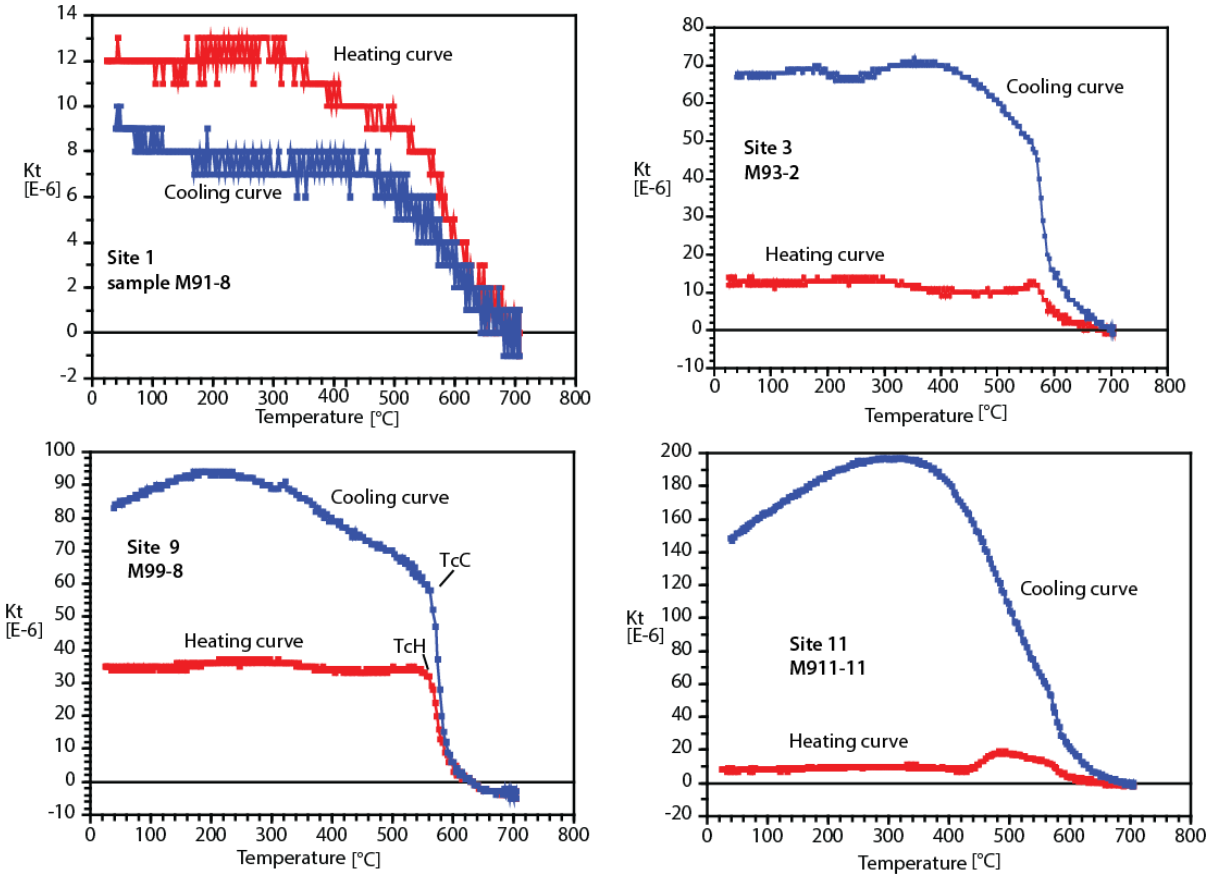

Figure 8: Results from Curie temperature tests on four example samples. TcH indicates the Curie temperature when heating, which is indicated by a sharp drop in susceptibility. TcC is the Curie temperature during cooling, and is the end of the steep increase in susceptibility during cooling. Most samples show some alteration during heating, evidenced by the higher susceptibility during cooling than heating, although this is not observed in site 1. Samples have Curie temperatures around 560 – 580°C, indicating that magnetite is the primary magnetic carrier. Site 3 shows a steepening in slope at around 650°C, which may indicate the presence of hematite.

5. Discussion

468 *5.1 Reliability of data*

469 Each palaeomagnetic site in the Zereg Basin was collected where the stratigraphy had been
470 previously determined and described in the literature (Devyatkin, 1981; Howard et al., 2003;
471 Khosbayar, 1973; Shuvalov, 1968, 1969; Sjostrom et al., 2001). Whilst we cannot place precise
472 age constraint on each locality, we can assign a geological period or epoch on the basis of the
473 previous work and sampling the same sections that other authors have documented. This
474 precision is sufficient for comparison with palaeomagnetic poles in the next section, which
475 are limited to the same level of precision as our lithostratigraphy.

476 Tilt correction of the sites results in better grouping of the mean directions, and directions
477 from all of the sites can be combined into a statistically significant fold test, positive at the
478 95% confidence level, using the classic McElhinny (1964) approach (Figure 9). During the fold
479 test site directions are incrementally restored back to horizontal from the stratigraphic
480 orientations, and α_{95} and K values are calculated for each 10% increment. If magnetic
481 directions in the samples have been reset since deposition and subsequent folding, the
482 scatter of the results (α_{95}) is predicted to worsen and the precision (k: essentially a measure
483 of the grouping of the data) will decrease, due to overprinting of the magnetisation on the
484 structure of the fold. If the directions are primary, the measures of precision and grouping
485 will improve, because the samples migrate to the 'true', tilt-corrected site mean.

Figure 9

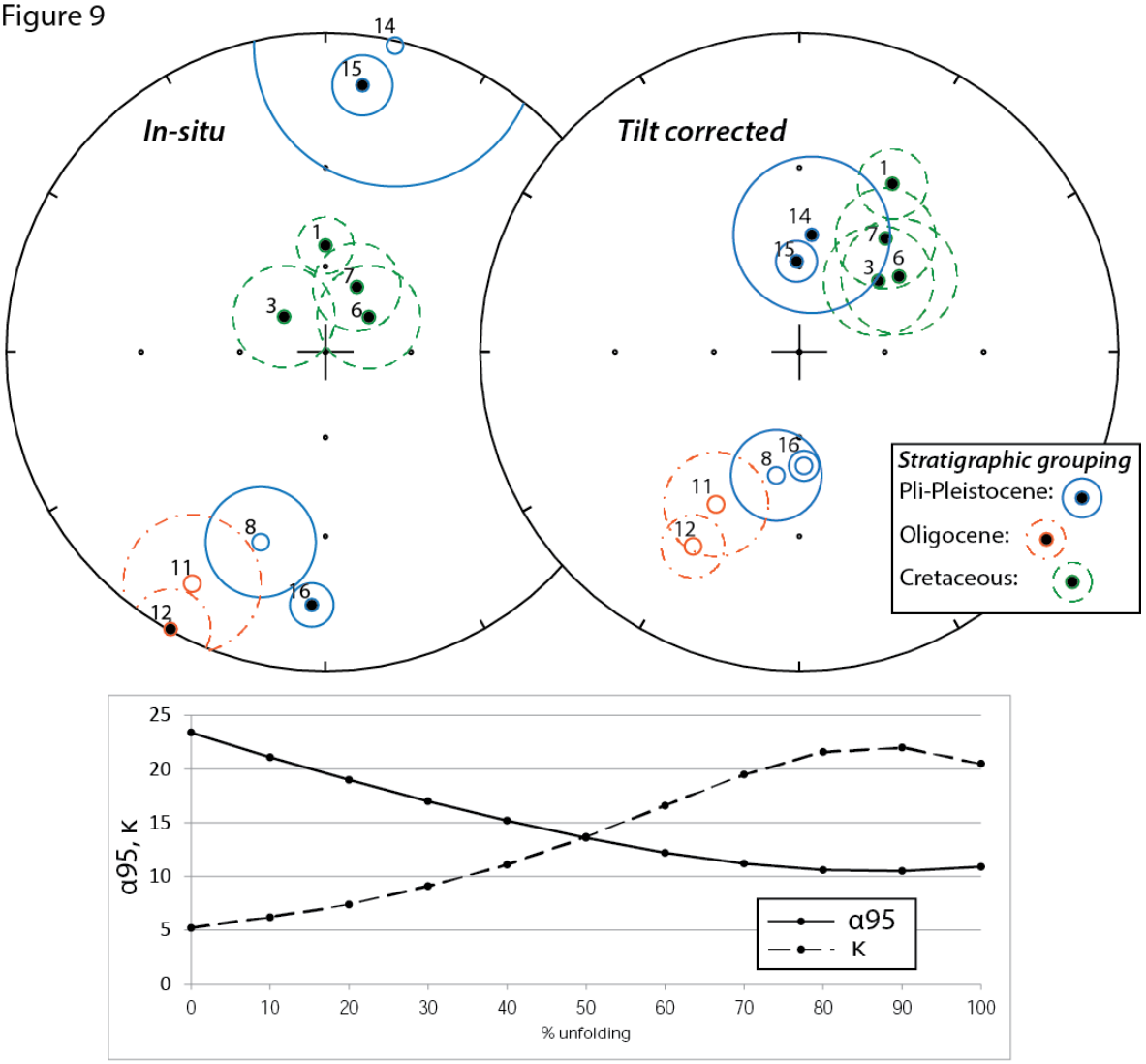

Figure 9: *In-situ* and tilt corrected site means and α_{95} cones of uncertainty are shown on the stereoplots (lower hemisphere projection) for all stable and consistent sites (site numbers are labelled). Closed circles indicate positive directions and open circles indicate negative directions, and all sites are plotted as a single (normal) polarity. The lower panel shows the results of the fold test that includes all sites, with a higher K value, indicating greater precision, with 90-100% unfolding.

Unfolding of the Zereg Basin sites by up to 90% results in a higher k value for the mean of all sites, which would not be the case if samples were remagnetised during or after tectonic tilting occurred. This positive fold test confirms that the isolated magnetic components are primary. Fold tests were also performed on groupings of the sites by age, but none of the groups produced a statistically significant fold test. This is likely because there is little

variability in bedding orientations within each age group, and the fold tests would be improved by sampling from units of the same age, but from strata with variable orientations.

Also attesting to primary magnetisation are several sites that have reversed polarity, exhibited in the Cenozoic sequences (Figure 9). While this is not necessarily confirmation of primary magnetisation, it does add confidence to the reliability of the directions because if overprinted, generally all samples will have the same polarity. Tilt-corrected directions are distinct from the present day field in the region, which has a north declination and a steep inclination of approximately 65°, suggesting that the measured directions are not the result of a present-day overprint. A steeply dipping, northerly overprint was found at low temperatures in several sites, but this component was removed by stepwise heading (e.g. sample M912-1, Figure 7, Oligocene group). Finally, the presence of significant shallowing of the inclinations is also supportive of a primary origin for the magnetization, because such shallowing occurs shortly after deposition during compaction and consolidation of the sediments.

5.2 Lack of rotation of the Zereg Basin

The mean palaeomagnetic directions measured from each of the Jurassic-Cretaceous, Oligocene, and Plio-Pleistocene sediments are displayed in Figure 10. The predicted declination and inclination for the samples, based on VGPs for stable Eurasia transformed to the Zereg basin locality, calculated from Torsvik et al. (2012), are also shown as squares on the same figure with dashed lines indicating the predicted declination. The mean inclinations are shallower than what is expected from the VGPs, confirming that some degree of flattening has occurred, probably as a result of compaction. The mean declinations are similar to those predicted by the VGPs, and even the oldest group is well within the 95% cone of uncertainty of the expected declination (Jurassic/Cretaceous D=40.6° ± 15.4°, compared to the VGP D=30.4° ± 3.0°). The Plio-Pleistocene grouping has the lowest uncertainty, and the mean declination is not rotated with respect to the expected declination (Pliocene D=003.4° ± 7.1°, compared to a VGP D=003.5° ± 3°).

The results from the Zereg Basin suggest that the region has not undergone a measurable amount of palaeomagnetic rotation since the deposition of the Jurassic/Cretaceous sediments. The results are of high quality, and pass several field tests that attest to primary

magnetisation, including reversal and fold tests. The ages of the strata are generally well defined, based on paleontological work, geologic mapping, and stratigraphy (Devyatkin et al., 1975; Howard et al., 2003; Sjostrom et al., 2001). The lack of rotation in the Zereg Basin is in strong contrast with both the existing palaeomagnetic results from the Chuya Basin in the Siberian Altay (Thomas et al., 2002), and with the anticlockwise rotations predicted by geodetic data and the pattern of faulting in the Altay (Bayasgalan et al., 2005; Cunningham, 2005). In the Chuya Basin, anticlockwise rotations of 39° ± 8° have been suggested on the basis of palaeomagnetic data from Oligocene and younger aged sediments, with reasonable tests of reliability. Even if a proportion of the rotation in the Chuya Basin is due to local basin-scale rotations, the contrast between palaeomagnetic results from the two localities in the Altay is significant.

Figure 10

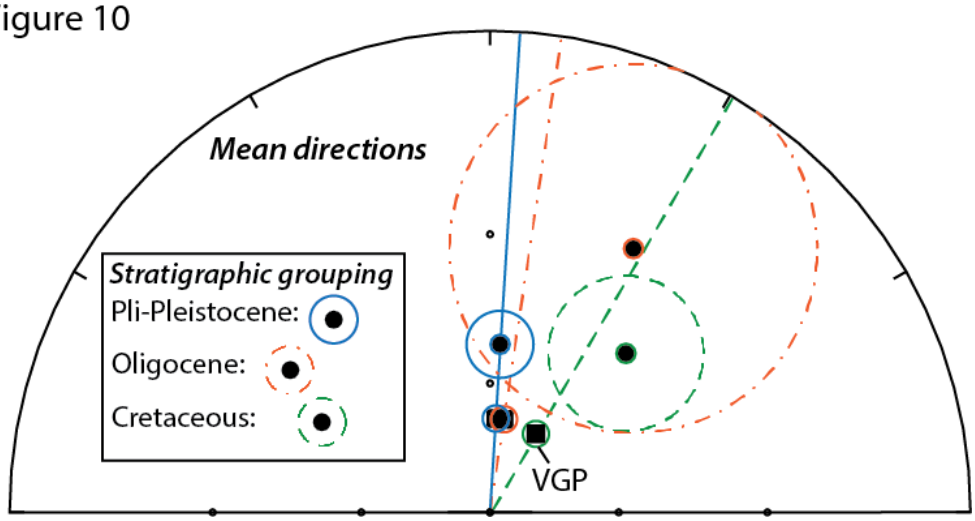

Figure 10: Age mean palaeomagnetic directions compared to the reference VGP poles we calculated for Mongolia (Torsvik et al., 2012). Our directions reflect some inclination shallowing but no rotation of the declination, within the error of the measurements.

Using the kinematic relationship in Walker and Jackson (2004), we can calculate a rotation rate for the Altay of 1.9˚ to 3.8˚ per million years, assuming that the faults slip on average 1-2 mm yr^{-1} and are spaced on average 30 km apart (*w* and *d* in figure 2, respectively). We also calculate the rotation rate in the Chuya Basin using the total rotation reported and the age (mid-Miocene and younger) of the sampled sediments. This is a minimum rate calculated with the assumption that rotation was ongoing as the sediments were deposited (e.g. if rotation initiated sometime after deposition, this would require the rotation rate to be faster).

550 Assuming a rotation of 39° and sediment age of 14 Ma, the rotation rate in Chuya would have
551 to be nearly 3° per million years, which agrees with the kinematic rotation rate of 1.9˚ to 3.8˚
552 calculated on the basis of the rate of fault slip and fault spacing. For comparison, we estimate
553 a maximum rate of rotation for the Zereg basin permissible by the resolution of our
554 palaeomagnetic data. The best-resolved mean direction comes from the Plio-Pliocene age
555 group, which has a 95% confidence window of 7˚ ((D=003.4° ± 7.1°, Figure 10). Therefore, the
556 Zereg basin must have rotated less than 7˚ since ~5 Ma, and the averaged rotation rate must
557 not exceed 1.4˚ degrees per Ma over that period. This can be accommodated either by having
558 a very young fault (less than 2.5 Ma) and rates comparable to those measured elsewhere in
559 the Altay (3˚ per million year as in the Chuya Basin), a significantly slower rate of rotation over
560 the time the fault is active, or some combination of these two scenarios.

561 Nissen et al. (2009b) estimate that the initiation age of the Har-Us-Nuur fault is 1.7-2.4 Ma
562 based on the Quaternary vertical displacement rate of 0.8-1.2 mm yr^{-1} and the vertical height
563 (2000 m) of the fault-bounded Jargalant Mountain, which is topped by a peneplain surface.
564 They assume that the initiation of faulting coincides with the onset of mountain building, as
565 the mountains are formed along restraining bends in the fault. Given the total offset-
566 constraints on the age of the fault, we favour the 'young fault' explanation for the lack of
567 observable rotation in the Zereg Basin, and therefore suggest this is indicative of the
568 expansion of the region of active faulting eastwards from the central Altay through time.
569 Using an initiation age of 1.7-2.4 Ma, we can infer a rate of anticlockwise rotation not
570 exceeding 2.9 – 4 degrees/Ma, with no lower bound.

571 The strike of the Har-Us-Nuur fault compared to other faults within the Altay is also indicative
572 of a shorter duration of activity and widening of the mountain range. The transpressional
573 Altay faults are characterised by anastomosing segments that on average strike NNW – SSE
574 (Figure 3). In general, fault segments that strike more northerly are dominated by strike-slip
575 motion. Segments that strike towards the west have a greater reverse component of slip, or
576 have at least developed branching reverse faults and flower structures (Figure 3;
577 Cunningham, 2005). Faults in the interior parts of the range trend more towards the west
578 (~314 – 330°), due to having a longer history of activity during which they accumulated more
579 anticlockwise rotation than the Har-Us-Nuur fault, which has a strike of 330 – 347°.

5.3 Implications for the timing and evolution of deformation in the Altay and central Asia

Thermochronologic studies from across the Altay are not in agreement on the initiation age of deformation in the region, and this has implications for the northwards propagation of the India-Asia collision. Many authors (e.g. Buslov et al., 2008; De Grave et al., 2007; Yin, 2010) reference young thermochronologic ages from the Altay and nearby Gobi Altay to imply that deformation has propagated over time and space northwards, through the Tien Shan and only recently into the Altay and Siberian plate margin. Apatite fission track (AFT) results from the Zereg Basin, some parts of the Siberian Altay, and the Gobi Altay place the initiation of deformation around 5 Ma, assuming that modelled cooling ages represent the onset of uplift of a widespread Jurassic planation surface preserved at the tops of mountains in these areas (De Grave et al., 2007; Jolivet et al., 2007; Vassallo, 2006). However both AFT and U-Th/He data from the Siberian part and central spine of the Altay hint at a longer-lived history of deformation, initiating sometime in the Oligocene to early Miocene (De Grave et al., 2007; Glorie et al., 2012a; Glorie et al., 2012b; Yuan et al., 2006). The central spine of the Altay also lacks a widespread planation surface, also suggesting that uplift may be more long-lived in this region, allowing more time for slow erosive processes to degrade the peneplain.

The lack of rotation measured in this study combined with the more recent thermochronologic data (Glorie et al., 2012a; Glorie et al., 2012b) supports a long-lived history of deformation in the Altay, with progressive widening of the range through time. This was first hypothesised by Nissen et al. (2009b), who suggested that older faults in the interior of the Altay rotate to less-favourable orientations and strain migrates outwards towards more favourably oriented structures and areas of lower topography to minimise the work done against gravity. Both the Har-Us-Nuur fault on the eastern margin of the range and the Fu Yun fault on the western margin strike more northerly (330 – 347°) and are thus inferred to be younger than faults in the high and compact central Altay mountains which on average strike more towards the west (~314 – 330°). Our palaeomagnetic data from the exterior of the range are in agreement with the hypotheses in Nissen et al. (2009b). It is likely that the major faults in the Altay have initiated as nearly pure strike slip faults, with a more northerly strike that followed the regional structural fabric and was not optimally-oriented with respect to the regional SH_{max} of the India-Asia collision. New faults were prone to anticlockwise rotation to accommodate the regional strain field, which placed them at a higher angle to SH_{max} as

611 rotation progressed. This encouraged the development of the flower structures present
612 across the central Altay which have branching reverse faults (e.g. Figure 3), because steeply
613 dipping strike-slip faults do not accommodate significant uplift. The evolving process of
614 deformation in the Altay has led to continuous mountain topography in the oldest parts of
615 the mountain range as structures coalesced. Strain partitioning in the Altay has not advanced
616 to the point such that the original generation of strike-slip faults have become inactive,
617 because there is clear evidence for neotectonic activity on strike-slip faults in the central part
618 of the mountain range (Frankel et al., 2010; Gregory et al., 2014), many of which do strike
619 more towards the north due to the anastomosing pattern of fault traces (Figure 3).

620 Other authors have used the lack of rotation measured on faults in central Asia to discuss
621 fault strength. van Hinsbergen et al. (2008) used the lack of rotation measured very close to
622 the Bogd fault in the Gobi Altay to suggest that the fault is weak, allowing strain to be localised
623 onto the fault, as otherwise they would have observed at least some local rotation. They also
624 suggest that strike-slip faulting in the range is subordinate to thrust faulting, despite the M
625 8.3 left-lateral strike slip earthquake that occurred in 1957 (see Figure 1 for the location of
626 the Bogd fault). However, in the case of the Bogd fault, rotation is simply not required by the
627 kinematics of faulting in the Gobi Altay, where fault strikes are aligned with the regional GPS
628 velocities (Figure 2), and so the lack of rotation cannot be used to infer fault strength.
629 Similarly, the lack of rotation we measure in this study cannot be used to comment on fault
630 strength because the lack of rotation on the Har-Us-Nuur fault is due to its young age of
631 initiation, and it has not been active for a sufficiently long time (e.g. > 5 m.y.) to have
632 accumulated measureable palaeomagnetic rotation.

633 **6. Conclusions**

634 We present the second palaeomagnetic study from Cenozoic rocks conducted in the Altay.
635 Samples collected from the Zereg Basin in the eastern Altay provide reliable palaeomagnetic
636 directions that pass a fold test and include a magnetic reversal. The declinations are not
637 significantly rotated with respect to the expected directions, which is in contrast with anti-
638 clockwise rotations of 39 ± 8° estimated from the Chuya Basin in the Siberian Altay. The lack
639 of palaeomagnetic rotations on the Har-Us-Nuur fault suggest that this fault is significantly
640 younger than the faults surrounding the Chuya Basin in the central Altay, and cannot have

641 rotated more than 7° in the past 5 m.y. Our work is in agreement with the young age of
642 initiation inferred by Nissen et al. (2009b; 1.7 - 2.4 Ma), and fits with the model of deformation
643 in the Altay where strike-slip faults progressively rotate as they accumulate displacement,
644 forming flower structures. Generally straight pure strike-slip faults striking closer to N-S are
645 younger than those with a more NW-SE orientation. This model is the result of strain being
646 accommodated on a pre-existing structural grain and rotating to accommodate regional
647 SH_{max}. The style of mountain building in the Altay is in contrast with compressional
648 deformation regimes across central Asia where thrust faulting dominates some mountain
649 belts (e.g. the Tien Shan), and left-lateral non-rotational shear arises elsewhere (e.g. the Gobi
650 Altay). More work is needed to unravel the relationship between the complexity of the
651 surface trace of faults where they have rotated, and how vertical axis rotation in general
652 influences the evolving pattern of deformation in an active transpressional mountain range.

653 **Tables**

654 **Table 1**: Palaeomagnetic sampling site localities, ages, and bedding orientations

655 **Table 2:** Site-averaged palaeomagnetic data and VGP comparisons (attached).

656 **Figures**

657 **Figure 1**: (a) SRTM shaded relief image of the Altay and (b) the India-Asia collision zone,
658 produced using the Generic Mapping Tools software (GMT, Wessel et al., 2013). In (a)
659 earthquake focal mechanisms are from Sloan et al. (2011), Nissen et al. (2007), and
660 Bayasgalan et al. (2005, other references within), with $M_w > 7$ events indicated. Active faults
661 are plotted in black (Baljinnyam et al., 1993; Gregory, 2012). (b) SRTM topography and major
662 tectonic boundaries of the India-Eurasia collision.

663

664 **Figure 2:** (a) SRTM shaded relief image of the Altay. GPS velocities are relative to stable
665 Eurasia and suggest ~7 mm yr^{-1} of northeast-directed shortening across the Altay (Calais et
666 al., 2006; Yang et al., 2008). Active faults are plotted in grey (Baljinnyam et al., 1993; Gregory,
667 2012). (b) Schematic diagram for deformation in Mongolia, with rotation on dextral faults in
668 the Altay (W Mongolia), and non-rotational shear required across the Gobi Altay and central

669 Mongolia, following the pattern of GPS-derived velocity vectors plotted in (a). In this
670 kinematic model, *w* indicates the average spacing between faults and θ is the degree of
671 rotation for an amount *d* of fault displacement after Walker and Jackson (2004) and described
672 in section 5.2.

673 **Figure 3:** Map of the Altay Mountains and active strike-slip faults. Black strain crosses show
674 the principal strain axes (compressional arrows point in, extensional arrows point out) from
675 Kreemer et al. (2014). Quaternary slip rates are noted in blue from Frankel et al. (2010);
676 Gregory et al. (2014); Nissen et al. (2009a); Nissen et al. (2009b); and Vassallo (2006). Rotation
677 estimates are plotted as rotational wedges in radians from north (white) with uncertainties
678 (grey) for the Chuya Basin (Thomas et al., 2002) and Zereg Basin (this study, each wedge
679 division is 2 radians). Coloured dots (earthquake locations) and arrows (earthquake slip
680 vectors) are for first-motion mechanisms (yellow; Bayasgalan et al., 2005, and references
681 therein), waveform-modelled solutions (red; Sloan et al., 2011, and references therein), and
682 from the Global CMT Catalogue (orange). Earthquake slip vectors are only plotted where the
683 fault plane is reliably established by field or remote mapping of the active trace. Where
684 discrimination between the fault and auxiliary plane is not possible, no slip vector is plotted.

685 **Figure 4**: (a) Landsat image (RGB = 741) of the Zereg Basin, with the three different sampling
686 localities indicated (North, North east, and South west). Figure 4 is indicated by dashed box.
687 Abbreviations are BHU: Baatar Hyarhan Uul, BU: Bumbat Uul, HF: Hovd Fault, HUN: Har-Us-
688 Nuur, HUNF: Har-Us-Nuur Fault, and JU: Jargalant Uul. The town of Zereg is indicated. (b) and
689 (c) are ASTER images of the northern and south-western sampling localities, with sample sites
690 labelled.

691 **Figure 5**: ASTER imagery (15 m/pixel) of the sampling sites from the northeast side of the
692 Zereg Basin. The lower panel shows a geological map of the area modified from Howard et al.
693 (2003) and (Nissen et al., 2009a), with the ages of the units mapped labelled and sampling
694 localities indicated. The region includes a syncline-anticline pair.

695 **Figure 6**: Photos of the exposures of Cenozoic and Mesozoic sediments in the northeast and
696 southeast Zereg Basin. (a) Outcrop of the upper red-bed unit, with strata uplifted by
697 southwest-dipping thrust faults (site 8). (b) Upper Red Bed Plio-Pleistocene sediments
698 uplifted on the flanks of Baatar Hyarhan Mountain, dipping SW towards the peaks of Baatar

Hyarhan in the background (sites 14-16). (c) Cretaceous sandstones with palaeomagnetic drill holes at site 6. (d) Oligocene Oasis Unit, with interbedded red sandstones (sampled, site 12) and yellow sandstones with cross bedding.

Figure 7: Example thermal demagnetisation Zijderveld diagrams from each rock unit sampled. Plots are shown tilt-corrected with a tectonic correction for the orientation of the strata sampled. Open points indicate the inclination, and closed points are the sample declination. North is to the right of the plot, and magnetic declinations are fit as vectors through measurements from high to low temperature.

Figure 8: Results from Curie temperature tests on four example samples. TcH indicates the Curie temperature when heating, which is indicated by a sharp drop in susceptibility. TcC is the Curie temperature during cooling, and is the end of the steep increase in susceptibility during cooling. Most samples show some alteration during heating, evidenced by the higher susceptibility during cooling than heating, although this is not observed in site 1. Samples have Curie temperatures around 560 – 580°C, indicating that magnetite is the primary magnetic carrier. Site 3 shows a steepening in slope at around 650°C, which may indicate the presence of hematite.

Figure 9: *In-situ* and tilt corrected site means and α_{95} cones of uncertainty are shown on the stereoplots (lower hemisphere projection) for all stable and consistent sites (site numbers are labelled). Closed circles indicate positive directions and open circles indicate negative directions, and all sites are plotted as a single (normal) polarity. The lower panel shows the results of the fold test that includes all sites, with a higher K value, indicating greater precision, with 90-100% unfolding.

Figure 10: Age mean palaeomagnetic directions compared to the reference VGP poles we calculated for Mongolia (Torsvik et al., 2012). Our directions reflect some inclination shallowing but no rotation of the declination, within the error of the measurements.

Acknowledgements:

LCG thanks the Oxford Clarendon Fund and Burdet-Coutts fund for support during her PhD. During this work, RTW was supported by the Royal Society of London through a University Research Fellowship, and TJC through a Research Fellowship from the Royal Commission for

the Exhibition of 1851. NERC is thanked for its support through NCEO/COMET and for supporting LCG through an Independent Research Fellowship. We thank Alex Densmore and Tony Watts for comments on an early draft of this manuscript, and three anonymous reviewers for constructive comments that improved the manuscript. We thank Nara, Deegi, and Amgaa for their valuable assistance in the field, and Bayasgalan Amgalan for his role in organising our fieldwork.

References

Abdrakhmatov, K.Y., Aldazhanov, S.A., Hager, B.H., Hamburger, M.W., Herring, T.A., Kalabaev, B., Makarov, V.I., Molnar, P., Panasyuk, S.V., Prilepin, M.T., Reilinger, R.E., Sadybakasov, I.S., Souter, B.J., Trapeznikov, Y.A., Tsurkov, V.Y., Zubovich, A.V., 1996. Relative recent construction of the Tien Shan inferred from GPS measurements of present-day crustal deformation rates. Nature 384, 450-453.

Badarch, G., Byamba, J., Mahbadar, T., Minjin, C., Orolmaa, D., Tomurtogoo, O., Khosbayar, T., 1998. Geological Map of Mongolia, in: Mineral Resources Authority of Mongolia, G.S. (Ed.). Mongolian Academy of Sciences, Institute of Geology and Mineral Resources, Ulaanbataar.

Badarch, G., Cunningham, W.D., Windley, B.F., 2002. A new terrane subdivision for Mongolia: implications for the Phanerozoic crustal growth of Central Asia. Journal of Asian Earth Sciences 21, 87-110.

Baljinnyam, I., Bayasgalan, A., Borisov, B.A., Cisternas, A., Dem'yanovich, M.G., Ganbaatar, L., Kochetkov, V.M., Kurushin, R.A., Molnar, P., Philip, H.e., Vashchilov, Y.Y., 1993. Ruptures of major earthquakes and active deformation in Mongolia and its surroundings, Geological Society of America Memoir. The Geological Society of America, pp. 1-61.

Bayasgalan, A., Jackson, J., McKenzie, D., 2005. Lithosphere rheology and active tectonics in Mongolia: relations between earthquake source parameters, gravity, and GPS measurements. Geophysical Journal International 163, 1151-1179.

Briggs, S.M., Yin, A., Manning, C.E., Chen, Z.-L., Wang, X.-F., 2009. Tectonic development of the southern Chinese Altai Range as determined by structural geology, thermobarometry, $^{40}Ar/^{39}Ar$ thermochronology, and Th/Pb ion-microprobe monazite geochronology. Geological Society of America Bulletin 121, 1381-1393.

Buslov, M.M., Kokh, D.A., De Grave, J., 2008. Mesozoic-Cenozoic tectonics and geodynamics of Altai, Tien Shan, and Northern Kazakhstan, from apatite fission-track data. Russian Geology and Geophysics 49, 648-654.

Calais, E., Dong, L., Wang, M., Shen, Z., Vergnolle, M., 2006. Continental deformation in Asia from a combined GPS solution. Geophysical Research Letters 33, L24319.

Calais, E., Vergnolle, M., San'kov, V., Lukhnev, A., Miroshnitchenko, A., Amarjargal, S., Deverchere, J., 2003. GPS measurements of crustal deformation in the Baikal-Mongolia area (1994-2002): Implications for current kinematics of Asia. Journal of Geophysical Research 108, 2501-2513.

Campbell, G.E., Walker, R.T., Abdrakhmatov, K.Y., Schwenninger, J.L., Jackson, J.A., Elliott, J.R., Copley, A., 2013. The Dzhungarian fault: Late Quaternary tectonics and slip rate of a major right-lateral strike-slip fault in the northern Tien Shan region. Journal of Geophysical Reasearch: Solid Earth 118, 5681-5698.

Cowgill, E., Arrowsmith, J.R., Yin, A., Xiaofeng, W., Zhengle, C., 2004. The Akato Tagh bend along the Altyn Tagh fault, northwest Tibet 2: Active deformation and the importance of transpression and strain hardening within the Altyn Tagh system. GSA Bulletin 116, 1443-1464.

773 Cunningham, D., Davis, S., Badarch, G., 2003a. Crustal architecture and active growth of the Sutai
774 Range, western Mongolia: a major intracontinental, intraplate restraining bend. Journal of
775 Geodynamics 36, 169-191.
776 Cunningham, D., Dijkstra, A., Howard, J., Quarles, A., Badarch, G., 2003b. Active intraplate strike-slip
777 faulting and transpressional uplift in the Mongolian Altai, Special Publications. Geological Society,
778 London, pp. 65-87.
779 Cunningham, W.D., 1998. Lithospheric controls on late Cenozoic construction of the Mongolian Altai.
780 Tectonics 17, 891-902.
781 Cunningham, W.D., 2005. Active intracontinental transpressional mountain building in the Mongolian
782 Altai: Defining a new class of orogen. Earth and Planetary Science Letters 240, 436-444.
783 Cunningham, W.D., 2007. Structural and topographic characteristics of restraining bend mountain
784 ranges of the Altai, Gobi Altai and easternmost Tien Shan, Geological Society, London, Special
785 Publications. The Geological Society of London, pp. 219-237.
786 Cunningham, W.D., 2011. Cenozoic normal faulting and regional doming in the southern Hangay
787 region, Central Mongolia: implications for the origin of the Baikal rift province. Tectonophysics 331,
788 389-411.
789 Cunningham, W.D., Windley, B.F., Dorjnamjaa, D., Badamgarov, G., Saandar, M., 1996. A structural
790 transect across the Mongolian Western Altai: Active transpressional mountain building in central Asia.
791 Tectonics 15, 142-156.
792 De Grave, J., Buslove, M.M., Van den haute, P., 2007. Distant effects of India-Eurasia convergence and
793 Mesozoic intracontinental deformation in Central Asia: Constraints from apatite fission-track
794 thermochronology. Journal of Asian Earth Sciences 29, 188-204.
795 De Grave, J., Van den haute, P., 2002. Denudation and cooling of the Lake Teletskoye Region in the
796 Altai Mountains (South Siberia) as revealed by apatite fission-track thermochronology. Tectonophysics
797 349, 145-159.
798 De Grave, J., Van den haute, P., Buslove, M.M., Dehandschutter, B., Glorie, S., 2008. Apatite fission-
799 track thermochronology applied to the Chulyshman Plateau, Siberian Altai, Region. Radiation
800 Measurements 43, 38-42.
801 Demarest, H.H., 1983. Error analysis for the determination of tectonic rotation from paleomagnetic
802 data. Journal of Geophysical Research 88, 4321-4328.
803 Devyatkin, E.V., 1981. The Cenozoic of Inner Asia stratigraphy, geochronology and correlation, in:
804 Nikiforova, K.V. (Ed.), Comb. Sov-Mongolian Sci. Res. Geol. Exped. Transactions, Nauka, Moscow. (In
805 Russian).
806 Devyatkin, E.V., Martinson, G.G., Shuwalov, V.F., Khosbayar, P., 1975. Stratigraphy of Mesozoic
807 deposits of Mongolia. The Joint Soviet-Mongolian Scientific Research Geological Expedition,
808 Leningrad, Nauka (in Russian) 13, 25-49.
809 Dupont-Nivet, G., Guo, Z., Butler, R.F., Jia, C., 2002. Discordant paleomagnetic direction in Miocene
810 rocks from the central Tarim Basin: evidence for local deformation and inclination shallowing. Earth
811 and Planetary Science Letters 199, 472-482.
812 England, P., Molnar, P., 1990. Right-lateral shear and rotation as the explanation for strike-slip faulting
813 in eastern Tibet. Nature 344, 140-143.
814 Fisher, R.A., 1953. Dispersion on a sphere. Proceedings of the Royal Society of London, Series A 217,
815 295-305.
816 Frankel, K.L., Wegmann, K.W., Bayasgalan, A., Carson, R.J., Bader, N.E., Adiya, T., Bolor, E., Durfey, C.C.,
817 Otgonkhuu, J., Sprajcar, J., Sweeney, K.E., Walker, R.T., Marstellar, T.L., Gregory, L.C., 2010. Late
818 Pleistocene slip rate of the Höh Serh-Tsagaan Salaa fault system, Mongolian Altai and intracontinental
819 deformation in central Altai. Geophysical Journal International 183, 1134-1150.
820 Gan, W., Zhang, P., Shen, Z.-K., Niu, Z., Wang, M., Wan, Y., Zhou, D., Cheng, J., 2007. Present-day crustal
821 motion within the Tibetan Plateau inferred from GPS measurements. Journal of Geophysical Research
822 112, B08416.

823 Glorie, S., De Grave, J., Buslov, M.M., Zhimulev, F.I., Elburg, M.A., Van den haute, P., 2012a. Structural
824 control on Meso-Cenozoic tectonic reactivation and denudation in the Siberian Altai: insights from
825 multi-method thermochronometry. Tectonophysics 544-545, 75-92.
826 Glorie, S., De Grave, J., Delvaux, D., Buslov, M.M., Zhimulev, F.I., Vanhaecke, F., Elburg, M.A., 2012b.
827 Tectonic history of the Irtysh shear zone (NE Kazakhstan): new constraints from zircon U/Pb dating,
828 apatite fission track dating and palaeostress analysis. Journal of Asian Earth Sciences 45, 138-149.
829 Gregory, L.C., 2012. Active Faulting and Deformation of the Mongolian Altay Mountains, Department
830 of Earth Sciences. University of Oxford.
831 Gregory, L.C., Thomas, A.L., Walker, R.T., Garland, R., Mac Niocaill, C., Fenton, C.R., Bayasgalan, A.,
832 Amgaa, T., Gantulga, B., Xu, S., Schnabel, C., West, A.J., 2014. Combined uranium series and ^{10}Be
833 cosmogenic exposure dating of surface abandonment: a case study from the Ölgiy strike-slip fault in
834 western Mongolia. Quaternary Geochronology 24, 27-43.
835 Howard, J.P., Cunningham, W.D., Davies, S.J., Dijkstra, A.H., Badarch, G., 2003. The stratigraphic and
836 structural evolution of the Dzereg Basin, western Mongolia: clastic sedimentation, transpressional
837 faulting and basing destruction in an intraplate, intercontinental setting. Basin Research 15, 45-72.
838 Jolivet, M., Ritz, J.F., Vassallo, R., Larroque, C., Braucher, R., Todbileg, M., Chauvet, A., Sue, C., Arnaud,
839 N., De Vicente, R., Arzhanikova, A., Arzhanikov, S., 2007. Mongolian summits: An uplifted, flat, old but
840 still preserved erosion surface. Geology 35, 871-874.
841 Khosbayar, P., 1973. New data on Upper Jurassic and Lower Cretaceous sediments of western
842 Mongolia. Academy of Sciences, USSR, Doklady (Earth Sciences Section) 208, 115-116.
843 Klinger, Y., Etchebes, M., Tapponnier, P., Narteau, C., 2011. Characteristic slip for five great
844 earthquakes along the Fuyun fault in China. Nature Geoscience 4, 389-392.
845 Kreemer, C., Blewitt, G., Klein, E.C., 2014. A geodetic plate motion and Global Strain Rate Model.
846 Geochemistry, Geophysics, Geosystems 15, 3849-3889.
847 Lukhnev, A.V., San'kov, V.A., Miroshnitchenko, A.I., Ashurkov, S.V., Calais, E., 2010. GPS rotation and
848 strain rates in the Baikal-Mongolia region. Russian Geology and Geophysics 51, 785-793.
849 McElhinny, M.W., 1964. Statistical significance of the fold test in palaeomagnetism. Geophysical
850 Journal of the Royal Astronomical Society 8, 338-340.
851 Meade, B.J., 2007. Present-day kinematics at the India-Asia collision zone. Geology 35, 81-84.
852 Merrill, R.T., McElhinny, M.W., McFadden, P.L., 1998. The Magnetic Field of the Earth. Academic Press.
853 Molnar, P., Ghose, S., 2000. Seismic moments of major earthquakes and the rate of shortening across
854 the Tien Shan. Geophysical Research Letters 27, 2377-2380.
855 Nissen, E., Emmerson, B., Funning, G., Mistrukov, A., Parsons, B., Robinson, D.P., Rogozhin, E., Wright,
856 T.J., 2007. Combining InSAR and seismology to study the 2003 Siberian Altai earthquakes--dextral
857 strike-slip and anticlockwise rotations in the northern India-Eurasia collision zone. Geophysical Journal
858 International 169, 216-232.
859 Nissen, E., Walker, R., Molor, E., Fattahi, M., 2009a. Late Quaternary rates of uplift and shortening at
860 Baatar Hyarhan (Mongolian Altai) with optically stimulated luminescence. Geophysical Journal
861 International 177, 259-278.
862 Nissen, E., Walker, R.T., Bayasgalan, A., Carter, A., Fattahi, M., Molor, E., Schnabel, C., West, A.J., Xu,
863 S., 2009b. The late Quaternary slip-rate of the Har-Us-Nuur fault (Mongolian Altai) from cosmogenic
864 ^{10}Be dates and luminescence dating. Earth and Planetary Science Letters 286, 467-478.
865 Scholz, C.H., Ando, R., Shaw, B.E., 2010. The mechanics of first order splay faulting: The strike-slip case.
866 Journal of Structural Geology 32, 118-126.
867 Sengör, A.M.C., Natal'In, B.A., Burtman, V.S., 1993. Evolution of the Altaid tectonic collage and
868 Palaeozoic crustal growth in Eurasia. Nature 364, 299-307.
869 Shuvalov, V.F., 1968. More information about Upper Jurassic and Lower Cretaceous in the southeast
870 Mongolian Altai. Academy of Sciences, USSR, Doklady (Earth Sciences Section) 197, 31-33.
871 Shuvalov, V.F., 1969. Continental redbeds of the Upper Jurassic of Mongolia. Academy of Sciences,
872 USSR, Doklady (Earth Sciences Section) 189, 112-114.

873 Sjostrom, D.J., Hendrix, M.S., Badamgarav, D., Graham, S.A., Nelson, B.K., 2001. Sedimentology and
874 provenance of Mesozoic nonmarine strata in western Mongolia: a record of intracontinental
875 deformation, Palaeozoic and Mesozoic tectonic evolution of Central and Eastern Asia: from
876 continental assembly to intracontinental deformation. Geological Society of America Memoir, pp. 361-
877 388.
878 Sloan, R.A., Jackson, J.A., McKenzie, D., Priestley, K., 2011. Earthquake depth distributions in central
879 Asia, and their relations with lithosphere thickenss, shortening and extension. Geophysical Journal
880 International 185, 1-29.
881 Tauxe, L., 2010. Essentials of Paleomagnetism. University of California Press.
882 Tauxe, L., Kent, D.V., 2004. A simplified statistical model for the geomagnetic field and the detection
883 of shallow bias in paleomagnetic inclinations: was the ancient magnetic field dipolar?, Timescales of
884 the Paleomagnetic field. American Geophysical Union, Washington, DC, pp. 101-115.
885 Thomas, J.C., Lanza, R., Kazansky, A., Zykin, V., Semakov, N., Mitrokhin, D., Delvaux, D., 2002.
886 Paleomagnetic study of Cenozoic sediments from the Zaisan basin (SE Kazakhstan) and the Chuya
887 depression (Siberian Altai): tectonic implications for central Asia. Tectonophysics 351, 119-137.
888 Thomas, J.C., Perroud, H., Cobbold, P., Bazhenov, M., Burtman, V.S., Chauvin, A., Sdybakasov, E., 1993.
889 A paleomagnetic study of Tertiary formations from the Kyrgys Tien-Shan and its tectonic implications.
890 J Geophys Res 98, 9571-9589.
891 Torsvik, T.H., Van der Voo, R., Preeden, U., Mac Niocaill, C., Steinberger, B., Doubrovine, P.V., van
892 Hinsbergen, D.J.J., Domeir, M., Gaina, C., Tohver, E., Meert, J.G., McCausland, P.J.A., Cocks, L.R.M.,
893 2012. Phanerozoic Polar Wander, Palaeogeography and Dynamics. Earth Science Reviews 114, 325-
894 368.
895 Van der Voo, R., 1989. Paleomagnetism of North America: The craton, its margins, and the
896 Appalachian Belt, in: Pakiser, L.C., Mooney, W.D. (Eds.), Geophysical Framework of the Continental
897 United States, Geol. SOC. Am. Mem. Geological Society of America, Washington, DC, pp. 447-470.
898 van Hinsbergen, D.J.J., Straathof, G.B., Kuiper, K.F., Cunningham, W.D., Wijbrans, J., 2008. No vertical
899 axis rotations during Neogene transpressional orogeny in the NE Gobi Altai: coinciding Mongolian and
900 Eurasian early Cretaceous apparent polar wander paths. Geophysical Journal International 173, 105-
901 126.
902 Vassallo, R., 2006. Chronologie et evolution des reliefs dans la region Mongolie-Siberie: approach
903 morphotectonique et geochronologique. L'Universite Montpellier II.
904 Vassallo, R., Jolivet, M., Ritz, J.F., Braucher, R., Larroque, C., Sue, C., Todbileg, M., Javkhlanbold, D.,
905 2007. Uplift age and rates of the Gurvan Bogd system (Gobi Altay) by apatite fission track analysis.
906 Earth and Planetary Science Letters 259, 333-346.
907 Walker, R., Jackson, J., 2004. Active tectonics and late Cenozoic strain distribution in central and
908 eastern Iran. Tectonics 23.
909 Walker, R.T., Bayasgalan, A., Carson, R., Hazlett, R., McCarthy, L., Mishler, J., Molor, E., Sarantsetseg,
910 P., Smith, L., Tsogtbadrakh, B., Tsolmon, G., 2006. Geomorphology and structure of the Jid right-lateral
911 strike-slip fault in the Mongolian Altay mountains. Journal of Structural Geology 28, 1607-1622.
912 Walker, R.T., Jackson, J.A., 2002. Offset and evolution of the Gowk fault, S.E. Iran: a major intra-
913 continental strike-slip system. Journal of Structural Geology 24, 1677-1698.
914 Walker, R.T., Nissen, E., Molor, E., Bayasgalan, A., 2007. Reinterpretation of the active faulting in
915 central Mongolia. Geology 35, 759-762.
916 Wang, Q., Zhang, P.-Z., Freymuller, J.T., Bilham, R., Larson, K.M., Lai, X.a., You, X., Niu, Z., Wu, J., Li, Y.,
917 Liu, J., Yang, Z., Chen, Q., 2001. Present-day crustal deformation in China constrained by Global
918 Positioning System measurements. Science 294, 574-576.
919 Weil, A.B., Sussman, A.J., 2004. Classifying curved orogens based on timing relationships between
920 structural development and vertical-axis rotations, in: Sussman, A.J., Weil, A.B. (Eds.), Orogenic
921 Curvature: Integrating Paleomagnetic and Structural Analyses: Geological Society of America Special
922 Paper, pp. 1-15.

Wessel, P., Smith, W., Scharroo, R., Luis, J., Wobbe, F., 2013. Generic Mapping Tools: Improved version released. EOS Transations AGU 94, 409-410.
Yang, S., Li, J., Wang, Q., 2008. The deformation pattern and fault rate in the Tianshan Mountains inferred from GPS observations. Science in China Series D: Earth Sciences 51, 1064-1080.
Yin, A., 2010. Cenozoic tectonic evolution of Asia: A preliminary synthesis. Tectonophysics 488, 293-325.
Yuan, W., Carter, A., Dong, J., Bao, Z., An, Y., Guo, Z., 2006. Mesozoic-Tertiary exhumation history of the Altai Mountains, northern Xinjiang, Chia: new constraints from apatite fission track data. Tectonophysics 412, 183-193.
Zhang, P.-Z., Shen, Z., Wang, M., Gan, W., Burgmann, R., Molnar, P., Wang, Q., Niu, Z., Sun, J., Wu, J., Hanrong, S., Xinzhao, Y., 2004. Continuous deformation of the Tibetan Plateau from global positioning system data. Geology 32, 809-812.
Zijderveld, J.D.A., 1967. AC demagnetization of rocks: analysis of results, Methods in Palaeomagentism. Elsevier, Amsterdam, pp. 245-286.
Zuza, A.V., Yin, A., 2016. Continental deformation accommodated by non-rigid passive bookshelf faulting: An example from the Cenozoic tectonic development of northern Tibet. Tectonophysics 677-678, 227-240.